Supplementary Information

Million-year-old DNA sheds light on the genomic history of mammoths

Tom van der Valk[1,2,3*], Patrícia Pečnerová[2,4,5*], David Díez-del-Molino[1,2,4*], Anders Bergström[6], Jonas Oppenheimer[7], Stefanie Hartmann[8], Georgios Xenikoudakis[8], Jessica A. Thomas[8], Marianne Dehasque[1,2,4], Ekin Sağlıcan[9], Fatma Rabia Fidan[9], Ian Barnes[10], Shanlin Liu[11], Mehmet Somel[9], Peter D. Heintzman[12], Pavel Nikolskiy[13], Beth Shapiro[14,15], Pontus Skoglund[6], Michael Hofreiter[8], Adrian M. Lister[10], Anders Götherström[1,16#], Love Dalén[1,2,4#]

1. Centre for Palaeogenetics, Svante Arrhenius väg 20C, SE-106 91 Stockholm, Sweden
2. Department of Bioinformatics and Genetics, Swedish Museum of Natural History, Stockholm, Sweden
3. Department of Cell and Molecular Biology, National Bioinformatics Infrastructure Sweden, Science for Life Laboratory, Uppsala University, Uppsala, Sweden
4. Department of Zoology, Stockholm University, SE-106 91 Stockholm, Sweden
5. Section for Computational and RNA Biology, Department of Biology, University of Copenhagen, DK-2200 Copenhagen, Denmark
6. The Francis Crick Institute, London NW1 1AT, UK
7. Department of Biomolecular Engineering, University of California Santa Cruz, Santa Cruz, CA, USA
8. Institute for Biochemistry and Biology, University of Potsdam, 14476 Potsdam, Germany
9. Department of Biological Sciences, Middle East Technical University, Ankara, Turkey
10. Department of Earth Sciences, Natural History Museum, London SW7 5BD, UK.
11. College of Plant Protection, China Agricultural University, Beijing 100193, China
12. The Arctic University Museum of Norway, UiT - The Arctic University of Norway, 9037 Tromsø, Norway
13. Geological Institute, Russian Academy of Sciences, Moscow, Russia
14. Department of Ecology and Evolutionary Biology, University of California Santa Cruz, Santa Cruz, CA, USA
15. Howard Hughes Medical Institute, University of California Santa Cruz, Santa Cruz, CA 96054 USA
16. Department of Archaeology and Classical Studies, Stockholm University, SE-106 91 Stockholm, Sweden

*) These authors contributed equally: Tom van der Valk, Patrícia Pečnerová, David Díez-del-Molino
#) These authors jointly supervised this work: Anders Götherström and Love Dalén
Correspondence: tom.vandervalk@scilifelab.se, love.dalen@nrm.se

Content

1. Sample description, morphology, and stratigraphy	3-10
2. DNA extraction and sequencing	10-12
3. Sequence data processing and mapping	12
4. Ancient DNA authenticity and quality assessment	12-14
5. Reconstruction of mitogenomes, tip-dating, and mtDNA phylogeny	15-16
6. Genetic age estimates based on autosomal data	16-18
7. Nuclear genetic relationships and phylogeny	19-20
8. D, f4-statistics, AdmixtureGraphs and TreeMix	21-25
9. Ghost admixture in Columbian and European mammoths	26-28
10. Genetic adaptations of the woolly mammoth	29-30
11. References	31-35

1. Description, morphology, and stratigraphy of Early-Middle Pleistocene samples

In this study we present genome data for three Early-Middle Pleistocene *Mammuthus* samples. The *Mammuthus* teeth designated here as Krestovka, Chukochya, and Adycha were recovered by the late Andrei Sher (Russian Academy of Sciences, Moscow) from three individual western Beringian Pleistocene mammal localities in the 1970s. The partial upper third molar PIN-3491-3 (described from here on as **Krestovka**) was discovered in 1973 in a cliff exposure along the right side of the Krestovka River at 68°08'14.4"N 157°44'56.5"E, 1.5 km from its junction with the Kolyma River. The intact last upper molar PIN 3341-737 (described from here on as **Chukochya**) was found in 1971 in a riverbank on the right side of the Bolshaya Chukochya River at Sher's site 35, 69°33'19.0"N 157°09'51.3"E. The fragmented lower third molar PIN 3723-511 (described from here on as **Adycha**) was recovered in 1976 from a gravel bar in the Adycha (or Adytcha in some literature) River at the locality named Oskhorkokh (or Oskordokh), at 67°31'46.7"N 135°41'15.0"E.

1.1. Dating of deposits yielding the mammoth teeth. The archaic morphological traits of the samples strongly suggest that they pre-date the late Middle Pleistocene[1–3] (Extended Data Fig. 1, Fig. S2). Only nine such early mammal localities are known in western Beringia, three of which comprise several individual sites[4,5]. Among these localities, Krestovka and Bolshaya Chukochya are the best-studied, being a major regional source of data on Early to Middle Pleistocene stratigraphy and fossil mammals. As samples Chukochya and Krestovka come from these highly informative localities, their age can be estimated with some confidence. As shown below, all three specimens belong to Lower (Early) or Upper (Late) Olyorian units of the regional stratigraphic scale (Extended Data Fig. 2). In view of the more ancient 'molecular clock' based estimates however (see main text), we discuss whether the age of the samples could be more ancient than that of layers from which they were recovered or to which they are logically attributed. In theory, some of the bones occurring in alluvial deposits could have been reworked from even more ancient deposits. Therefore, in what follows, we additionally consider the most ancient localities of western Beringia. Their chronology may constrain the maximum conjectural age of the finds. Concerning deposits pre-dating the late Middle Pleistocene throughout western Beringia, biostratigraphy and magnetostratigraphy are the leading methods for chronological control, as well as local and global correlation of the lithostratigraphic units. Recent advances in direct dating of tephra (volcanic ash) and basalts in neighbouring eastern Beringia (Alaska/Yukon) have confirmed previous chronological estimates made on the basis of biostratigraphy and palaeomagnetism. In the current research we do not use mammoth-taxonomy-based biochronology[6] to avoid possible circular arguments. The regional fossil record has been examined in depth since it was proposed to be, and then became, the basis for establishing Land Mammal Ages and Horizons (Regional Stages of the Regional Stratigraphic Scale) for a substantial part of western Beringia[7]. Three sequential, though not necessarily stratigraphically concatenate, pre- late Middle Pleistocene mammal faunas were revealed in western Beringia (Extended Data Fig. 2). In decreasing chronological age they comprise the Kutuyakhian, Early Olyorian, and Late Olyorian[1,4,8–10]. Another fauna, designated here as the *Phenacomys* complex, has been described in several studies[1,4,11], but has never been treated as a distinct biostratigraphic unit as it came from a separate, poorly studied locality that lacks clear evidence

of its stratigraphic position. New evidence suggests the evolutionary grade of species within the *Phenacomys* complex is intermediate between that of the Kutuyakhian and Early Olyorian. Thus, the *Phenacomys* fauna provides valuable insights for the current discussion.

1.2. Kutuyakhian - the earliest west Beringian fauna and age of the Kutuyakh beds. The earliest late Cenozoic mammals ever recorded in northeastern Asia, ranging down to at least 60 degrees north, come from the Kutuyakh beds of Sher's Krestovka locality 6 (the Krestovka specimen was recovered from the same locality, but within a higher stratigraphic unit). There are indirect indications that mammals older than Kutuyakhian will never be found in western Beringia, neither *in situ* nor reworked. Although pre-Kutuyakhian Cenozoic terrestrial deposits are known in western Beringia, despite massive efforts not even a tiny fragment of mammal bone has ever been discovered within them. Conversely, they are often abundant in plant fossils. This could be because of past climate-induced taphonomy. Macroscopic plant, pollen and lithological evidence suggests the climate in western Beringia before Kutuyakhian times was much warmer and more humid than subsequently[4,12]. This led to acidic geochemical environments, highly unfavorable for bone preservation, but good for plant remains. An illustrative, though extreme, current example of such environments is the north-European peat bogs. Numerous ancient human mummies have been found there, often completely lacking the mineral constituent of bones due to dissolution[13]. The Kutuyakhian rodent fauna is relatively abundant, yet large mammals are limited to a fragment of reindeer limb bone, and even here its provenance has been questioned[1]. The Kutuyakh Beds in general are reversely magnetized although they are normally polarised at their base and within a short interval in the upper sequence[14]. The Kutuyakh fossils come only from the reversely-magnetized upper portion of the beds. The Matuyama Chron (2.59-0.78 Ma) is the only long-term episode of reversed magnetization to which Kutuyakh mammals may correlate, considering their evolutionary position[11]. In principle, the Kutuyakh Beds' palaeomagnetic pattern could fit either within the lower half of the Matuyama Chron preceding the positive Olduvai Subchron (1.95-1.78 Ma), or the upper part of the Chron that includes some portion of the Olduvai, the long reversely magnetized interval above it, and the short positive Cobb Mountain episode at ca. 1.2 Ma (Extended Data Fig. 2). Detailed biostratigraphy further constrains the Kutuyakh chronology. The Kutuyakhian small mammal fauna includes *Ochotona* ex. gr. *collaris*, *Mimomys* cf. *coelodus*, *Cromeromys* cf. *irtyshensis*, and *Synaptomys* (*Plioctomys*) sp.[11] (Fig. S1). This relatively high latitude complex can barely be directly assigned to the Central and South European Small Mammal Biozones (MN/MQ and or MNR/MQR). It reliably correlates with them, however, through a number of faunal complexes known in West Siberia and in Central, Eastern, and Northwestern Europe. Central and Eastern European *Synaptomys* is referred to the Early Villafranchian (ca. 3.5 – 2.6 Ma). The Kutuyakhian *Synaptomys* is more advanced, and considering paleomagnetic data suggests an age between 2.5 and 2.0 Ma[11]. The evolutionary sequence of Late Cenozoic small and large mammal faunas in southwest Siberia is well-studied[15]. Important is that European and southwest Siberian records share many common taxa. This has made it possible, together with palaeomagnetic control, to tightly correlate southwest Siberian faunas with European Small Mammal Biozones (MN/MQ, MNR/MQR) and European Land Mammal Ages (ELMA). Based on small mammals, earlier research[11,16] has demonstrated an isochrony of the Kutuyakhian fauna with those recovered from the Podpusk-Lebyazhye Beds of Podpusk and Lebyazhye in southern

West Siberia. At Lebyazhye, the bone-bearing layer is also reversely magnetized (base of the Matuyama Chron) and overlays positively magnetized deposits, interpreted as Gauss Chron, that contain a more primitive mammal fauna[17]. This all led to one conclusion: that the Podpusk-Lebiazhie and consequently Kutuyakhian faunas best correlate to European faunas dated to the lowest part of the Matuyama Chron, some 2.5 – 2.0 Ma[11]. The position of the Kutuyakhian fauna in the global time scale is further supported, and more precisely dated, by data from Northern Europe. The key benchmark here is the biostratigraphic sequence obtained from the Zuurland (Brielle, the Netherlands) drilling project[18]. A comprehensive record of small mammals spanning the last 2.5 Ma has been obtained here[18,19]. Based on the evolutionary sequence of arvicolids (water voles), five major biostratigraphic units were recognized in the Zuurland sequence (Units ZU-5 to ZU-1) ranging from the earliest Pleistocene (Gelasian) to the Holocene[18–20] (the stratigraphic position of units ZU-5 to ZU-3 is shown in Extended Data Fig. 2). The Late Villanyian ZU-5 fauna correlates to an early stage of the MN17 biozone, which is placed at the beginning of the Pleistocene (i.e. with a lower bound at 2.59 Ma). Even more precisely, based on the evolutionary position of *Cromeromys* and *Synaptomys* from the Kutuyakhian, Tesakov (personal communication) correlates the Kutuyakh to the transition between the MNR3 and MNR2 biozones[21], that is at 2.45 Ma. These independent lines of evidence suggest the age of the Kutuyakh fauna and its source beds are bracketed in the range 2.50-2.45 Ma (Extended Data Fig. 2). The important conclusion is that in any event the Kutuyakhian is no older than 2.59 Ma since neither the fossil-bearing part of the Kutuyakh beds nor correlative horizons in Northern Eurasia cross the Gauss-Matuyama palaeomagnetic boundary.

1.3. *Phenacomys* complex. In the 1970s, within alluvial lenses at the base of a small isolated outcrop (Locality 8 of the Krestovka River), Andrei Sher found a peculiar fauna that included small and large mammals: derived *Phenacomys* described as *Phenacomys* sp., *Cromeromys* cf. *intermedius*, *Equus (Plesippus)* sp., and Ovibovini gen. indet.[1,4,11] (Fig. S1). This fauna appeared to be more advanced than Kutuyaknian and less advanced than Early Olyorian[11]. The exact stratigraphic position of the fauna-bearing beds was hard to determine. The locality is several kilometers from the well-studied Krestovka localities, the fossiliferous beds were poorly exposed, and no stratigraphic relations with units of known age could be revealed. A palaeomagnetic study by Virina *et al.*[14], however, showed the beds to be positively magnetized. Combining this fact with the proposed evolutionary position of the *Phenacomys* taxa (Tesakov, personal communication 2020), the fauna and the fossiliferous lens were eventually correlated to the Olduvai Subchron (1.95-1.78 Ma) (Extended Data Fig. 2).

1.4. Early Olyorian fauna and age of the Lower Olyorian unit. The Early Olyorian fauna, known from many localities throughout western Beringia, is abundant and diverse. It is now known to include more than 25 taxa of large and small mammals, many of which are biostratigraphically significant[10]. Chronological constraints on the Early Olyorian fauna and the Lower Olyorian stratigraphic unit have now been supported by many independent lines of evidence. At a coarse stratigraphic level, the evolutionary position of small and large mammals correlates the Lower Olyorian beds with the upper half of the Matuyama Chron (~1.5-0.78 Ma)[9,10]. Palaeomagnetism and correlation with well-dated northern North American faunas (from Yukon Territory and Alaska)

provide more exact and reliable age constraints. The mostly reversely-magnetized Lower Olyorian beds start slightly beneath a short-term positive paleomagnetic episode interpreted to be the Jaramillo Subchron (1.07 – 0.99 Ma)[4,14]. The Early Olyorian is younger than the fossiliferous lens at Old Crow CRH94 locality (Yukon Territory): the latter contains *Predicrostonyx hopkinsi* that is the basal taxon in the collared lemming lineage (Harrington, 2011) whereas the Early Olyorian fauna contains its immediate successor *Predicrostonyx compitalis*[11] (Fig. S1). The CRH94 beds have a layer of tephra, named Little Timber, which was dated by the fission-track method to 1.37±0.12 Ma[22]. So the Early Olyorian is younger than 1.37±0.12 Ma. The Early Olyorian is also younger than the Cape Deceit fauna recovered from the Cape Deceit locality in Alaska[23], as inferred from the following evidence. All Early Olyorian taxa are close to, but still somewhat more advanced than, those from Cape Deceit (Zazhigin, personal communication 2020). Importantly, the Cape Deceit fossiliferous lens is normally magnetized[24]. Storer[25] interpreted this positive episode as a correlate of the Olduvai Subchron (1.95 – 1.78 Ma), which corresponds to[4], or is older than[26], the age estimate of earlier authors based on biostratigraphic data. After the Cape Deceit assemblage had been examined in depth, however, it became evident that it is mixed[25]. Of critical significance are rodent morphotypes that are more advanced than those from the accurately-dated Fort Selkirk fauna (Yukon Territory)[25]. The Fort Selkirk mammal-bearing deposits are independently dated by $^{40}Ar/^{39}Ar$ and fission-track methods to 1.7-1.5 Ma[27,28], that is well above the Olduvai Subchron. Therefore, the positively magnetized Cape Deceit deposits contain fossils that are younger than 1.7-1.5 Ma and might correlate to the Cobb Mountain normal polarity palaeomagnetic episode (1.20 - 1.19 Ma). Summing all of these data we can conclude that the lower age of the Lower Olyorian is between 1.2-1.07 Ma (Extended Data Fig. 2). The upper age constraint of the Lower Olyorian is roughly defined by the beginning of the Upper Olyorian, since despite some sedimentation break recorded between the two parts of the Olyorian, the morphological differences between the most derived Early Olyorian taxa and their Late Olyorian representatives are relatively minor[1,10]. As will be shown below, the Upper Olyorian starts just below the Matuyama-Brunhes paleomagnetic reversal, about 0.8 Ma (Extended Data Fig. 2).

1.5. Late Olyorian fauna and age of the Upper Olyorian unit. The Late Olyorian fauna is also rich and well-represented. Upper Olyorian sediments containing the Late Olyorian fauna overlay the Lower Olyorian with a not always explicit unconformity. However, palaeomagnetic data combined with biostratigraphy clearly imply some sedimentary break. At the very base of the Upper Olyorian unit within its stratotype at the Krestovka River, the magnetic polarity turns from reversed to normal[14]. This reversal is clearly interpreted as the Matuyama-Brunhes boundary since, at the same stratigraphic level, the typical early Middle Pleistocene collared lemming *Dicrostonyx renidens* first occurs. This stratigraphic position is independently confirmed by the simultaneous presence of advanced forms of *Allophaiomys* cf. *pliocaenicus* (= *A. reservatus* Zazhigin) and archaic *Microtus* at the very base of the Upper Olyorian beds (Fig. S1), in the still reversely-magnetized part of it[11]. The exact age of the Late Olyorian termination is unknown. It is roughly estimated at 0.6 - 0.5 Ma, since there are considerable differences between the Late Olyorian and the next known (late Middle Pleistocene) rodent fauna in the region. More precise information came from the Bolshoy Khomus-Yuriakh locality 83 in arctic Siberia[9]. A transitional form between Late Olyorian *Dicrostonyx renidens* and presumed descendant (known to be post-

Olyorian) taxon *D. simplicior* has been recovered from here (Sher, personal communication; Zazhigin, personal communication). ^{36}Cl/Cl dates suggest an age of more than 0.4 Ma for this horizon that contains the transitional form[29]. So, the Upper Olyorian likely extends no later than 0.5 Ma (Extended Data Fig. 2).

1.6. Age of the Krestovka specimen: onset of Early Olyorian and possibility of pre-Olyorian age. According to Sher's field records, the Krestovka molar was recovered *in situ* from Krestovka site 6, within the basal bone-bearing lens of the Lower Olyorian unit. It is uncertain from which of the excavation trenches, spaced many dozens of meters apart along Location 6, the specimen was recovered. In some of the trenches, the basal lenses contain reworked *Phenacomys* and probably even Kutuyakhian mammal taxa, but other trenches lack any noticeable reworked material[4]. This makes a pre-Olyorian age for the Krestovka specimen at least possible. We assume, however, that the specimen was not reworked since it is not rolled and has no other signs of ancient redeposition: peculiar color, excessive mechanical destruction or chemical dissolution. Thus, its age is highly likely constrained to the very onset of the Early Olyorian (c. 1.2 - 1.1 Ma) (Extended Data Fig. 2). If the specimen after all was reworked from *Phenacomys* beds, the Kutuyakhian, or some other, no longer existing pre-Olyorian horizon (for which we have no evidence), the age constraint could spread down to some 1.8 or even 2.2 - 2.5 Ma, though not earlier. This scenario is, however, highly hypothetical since no mammoth remains are reliably recorded from either the Phenacomys beds or the Kutuyakhian.

1.7. Late Olyorian age of the Chukochya specimen. Following Sher's field report, the Chukochya specimen was found eroding from the base of a cliff exposure at B. Chukochya site 35. Extensive screen-washing of loose sediment was accomplished here in the 1970s to early 1990s, yielding a rich rodent fauna. The variation of rodent morphotypes in the sample appeared to be very low which excludes mixing of deposits and suggests a narrow time-interval (Zazhigin, personal communication 2020). The rodent taxonomic composition, comprising *Dicrostonyx renidens* and *Microtus* sp., clearly suggests a Late Olyorian age (0.8 - 0.5 Ma) for the mammal-bearing deposits and, therefore, the Chukochya specimen. Hypothetically, it is possible the mammoth specimen was relocated here from site 34, which is only a few dozens of meters upstream from site 35. This could have happened in Early Pleistocene times during common alluvial processes, or recently due to, for example, ice-rafting to the present position during the spring ice break. In this case an Early Olyorian age (1.2 – 0.8 Ma) of the specimen is not impossible since biostratigraphy and especially the palaeomagnetic pattern clearly indicate Lower Olyorian at site 34[4,14]. This scenario is, however, also entirely hypothetical in the absence of evidence.

1.8. Surface Oskordokh locality: age constraints for the Adycha specimen. The age of mammal remains recovered from the Oskordokh locality, including specimen Adycha, is hard to determine precisely, since it is a gravel bar lacking any pre-Late Pleistocene exposures nearby. The closest, and the only one yielding useful stratigraphic context, is Ulakhan-Sullar, 18 km downstream from Oskordokh. However, the Oskordokh locality is famous for the frequent occurrence of ancient mammal bones. New fossil discoveries are made here every year due to

seasonal water reworking of the gravel bar and reworking from the channel during spring flooding. Typical Early Olyorian and Late Olyorian mammal fossils have been recovered from the Oskordokh locality in quantity. According to detailed research by one of us (Pavel Nikolskiy; PN), mammals pre-dating the Early Olyorian have never been found here. At the Ulakhan-Sullar locality, which was last surveyed by PN in 2019, a definite Upper Olyorian unit is recorded, but no evidence of *in situ* Lower Olyorian has been revealed so far. Instead, both small mammals and palaeomagnetic data[30] exclude *in situ* Lower Olyorian here. Redeposited remains of both small and large mammals (such as early ~1 Ma *Cervalces*, early *Equus (Plesippus)* sp. and *Mimomys*) occur here sporadically. The morphologically “ancient-looking" taxa from Oskordokh are much akin to the *ex situ* Early Olyorian elements of the Ulakhan-Sullar fauna. In sum, the Oskordokh Adycha specimen is very probably Early or Late Olyorian in age. Only hypothetically could it be pre-Olyorian (down to Kutuyakhian age). Its likely age range is between 1.2-0.5 Ma, but 1.2 – 1.0 Ma is more probable.

			Mimomys cf. *coelodus*	*Cromeromys* cf. *irtyshensis*	*Synaptomys* (*Plioctomys*) sp.	*Phenacomys* sp.	*Cromeromys* cf. *Intermedius*	*Allophaiomys* cf. *Pliocaenicus*	*Lemmus sheri* Abramson, 1992	*Predicrostonyx compitalis* Zazhigin, 1976	*Allophaiomys* sp.	*Lemmus* cf. *obensis*	*Dicrostonyx renidens* Zazhigin, 1976	*Microtus* spp.
Fauna-bearing stratigraphic units	Upper Olyorian	Main										+	+	+
		Lowermost									+	+	+	
	Lower Olyorian							+	+	+				
	Phenacomys complex					+	+							
	Kutuyakhian		+	+	+									

Fig. S1. Presence-absence matrix for the arvicoline rodent species in deposits pre-dating the late Middle Pleistocene throughout Krestovka and Chukochya (western Beringia), adapted from Zazhigin *et al.*[11].

1.9. Morphometry of mammoth molars. Mammoth molars were measured according to the method of Lister & Sher (supplementary materials)[3]. Samples considered are as follows: *Mammuthus meridionalis*, ca. 2.0 Ma, Upper Valdarno, Italy (type locality) (n= 34); *M. trogontherii*, ca. 0.6 Ma, Süssenborn, Germany (type locality) (n=48); *M. primigenius*, Late Pleistocene (mostly ca. 45-15 ka) of Yana-Kolyma lowland, NE Siberia (Russia) and Alaska (USA) (n=28). Early (n=8) and Late (n=15) Olyorian samples are from localities in the Yana-Kolyma lowland (Early Olyorian is ~1.2 – 0.8 Ma, Late Olyorian is 0.8 – 0.5 Ma). North American Early to early Middle Pleistocene samples (ca. 1.5 – 0.5 Ma) are from Old Crow (Yukon, Canada), Leisey Shell Pit 1A and Punta Gorda (Florida, USA), and the Ocotillo Formation (California, USA) (combined n=16). Original data are from [3] Tables S1, S2), where further details on sites and collections can be found.

The crown of a mammoth molar comprises a series of enamel lamellae ('plates'), filled with dentine and held together by cement (Fig. S2). Last molars (upper and lower M3) are preferred for biometric comparisons because they are easily identifiable from their diagnostic shape, and they show the most marked evolutionary changes. The key molar parameters in the evolution of the mammoth lineage are the height of the unworn crown (hypsodonty) and the number of lamellae in the molars, both of which broadly increase through time; and the thickness of the enamel, which broadly decreases. Hypsodonty significantly increases the volume of the molar, allowing the animal to take more abrasive food without shortening its lifespan through an increased rate of tooth wear, while lamellar increase and thinning increases the efficiency of processing smaller leaf sizes (grass). Molar evolution in the mammoth lineage is broadly correlated with a shift from browsing (tree/shrub diet) to grazing (grass and other low-growing plants), because of increased rate of tooth wear from the higher silica and fibre content of grass and/or a greater quantity of grit and dust picked up during low feeding[31,32].

Because fossil molars are often incomplete, the lamellar frequency (a measure of density of lamellar packing) or its inverse, the average length of a lamella, are used as proxies for total lamella number. For upper molars, with parallel lamellae, lamellar length values are averaged between top and bottom of the crown. For lower molars, lamellae converge toward the top of the crown; so to avoid wear-dependent variation, only measurements taken at the base of the crown are used. Moreover, because of likely positive correlation of all parameters with crown size, they are generally plotted against a measure of molar size (crown length or width) or are normalised for size. Here the latter is achieved by dividing by crown width to obtain the hypsodonty index (crown height/width), lamellar length index (average lamellar length/crown width), and enamel thickness index (average enamel thickness/crown width). Separate graphs are plotted for upper and lower M3 because of their shape differences; here, Krestovka and Chukochya are upper M3s and Adycha is a lower M3 (Extended Data Fig. 1). For upper M3s, both Krestovka and Chukochya are measurable on both critical parameters of hypsodonty and lamellar length, so a bivariate plot of these variables is shown. For lower M3s, the molar is too worn for accurate measurement of hypsodonty, so lamellar length and enamel thickness are plotted.

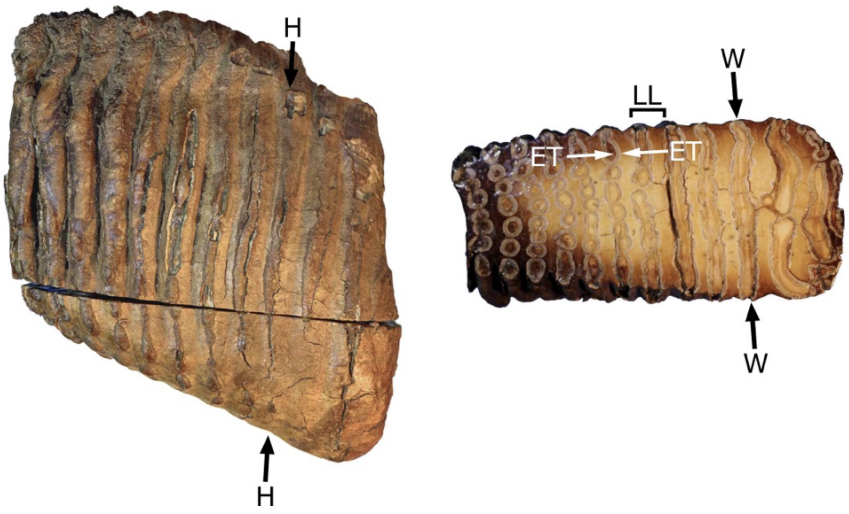

Fig. S2. side (left) and occlusal (right) views of upper M3 of the Krestovka specimen showing measurement positions: W = crown width, H = crown height, LL = lamellar length, ET = enamel thickness.

2. DNA extraction, library preparation, and sequencing

Samples from the ancient mammoth molars (Krestovka, Adycha, Chukochya) were processed in the clean ancient DNA laboratories at the Swedish Museum of Natural History and at the Centre for Palaeogenetics in Stockholm. The ancient DNA laboratories have HEPA-filtered air intakes and positive air pressure, and are physically separated from the buildings housing post-PCR laboratories. Standard procedures of working with degraded and ancient samples were followed, including wearing protective clothing, masks, and gloves, frequent sterilization of surfaces and tools, and using negative controls. Since our samples consisted of small subsamples, we could only select the best section for drilling locally. We targeted sections of the teeth that seemed the least weathered, with dense consistency, while avoiding visible cracks, along which bacteria can enter. Moreover, in order to remove potential surface contamination, the surface layer of a tooth was removed using a Dremel drill in the section where we aimed to perform the final drilling. After this, the drill bits and tinfoil were changed and the hood surface was sterilized with sodium hypochlorite. The fine powder used for the DNA extraction was obtained by drilling towards the interior part of the tooth and the drilling speed was kept low to avoid overheating and damaging the DNA. Approximately 50 mg of tooth powder was collected and used to extract DNA following the protocol described in Dabney *et al.*[33], which is optimized for the recovery of short DNA fragments. Illumina compatible double-stranded DNA libraries were constructed for all samples from 20 µL of DNA extract following the established protocol by Meyer & Kircher[34] and incorporating USER-enzyme (New England Biolabs) treatment as described in Pečnerová *et al.*[35]. The library build consisted of blunt-end repair (with 6 µL of USER enzyme), adapter ligation, and adapter fill-in, with cleaning steps in between performed using MinElute Purification Kit (Qiagen) and elution volume of 40 µL. Libraries were single-indexed and amplified from 3 µL of library template using 12 to 16 amplification cycles. After initial screening of sequencing libraries, an additional three and four extracts were prepared for samples Adycha and Krestovka, respectively, from newly drilled tooth powder, following the same protocol, and new libraries were built for all

samples. Additional libraries from sample Adycha were single-indexed, whereas the additional libraries from sample Krestovka were dual-indexed. For deep-sequencing, libraries for all three specimens were indexed using a reduced number of amplification cycles (8 to 12) in a number of independent reactions to minimize clonality (Table S1). Indexed libraries were purified along with size selection using Agencourt AMPure XP beads (Beckman Coulter) and their concentrations were measured with a high-sensitivity DNA chip on a Bioanalyzer 2100 (Agilent). Libraries from each individual were pooled in equimolar ratios to obtain one separate pool for each individual, and these were subsequently sequenced on full, separate lanes of the Illumina platform at the Science for Life Laboratory (SciLifeLab, NGI Stockholm). Six HiSeqX lanes (2x150 base pair (bp) mode) were used for sample Adycha, and two lanes for sample Chukochya. The Krestovka sample was sequenced on one lane on the Illumina HiSeqX platform in paired-end 2x150 bp mode, and half an S4 lane on the Illumina NovaSeq6000 platform in paired-end 2x150 bp mode.

We also analysed two Late Pleistocene woolly mammoth samples from Europe (Scotland) and Siberia (Kanchalan), obtained from museum collections. The Scotland sample (ID: V5123, Hunterian museum) originates from the Kilmarnock area, Scotland, while the Kanchalan sample (ID: 4-010, North-East Interdisciplinary Scientific Research Institute n. a. N. A. Shilo, Far East Branch, Russian Academy of Sciences, Magadan, Russia) originates from South Chukotka, Russia. These samples were processed in the ancient DNA laboratory in the University of York. For both samples, an area of the larger tusk was cleaned with the Dremel drill bit, and a small piece removed and ground with a pestle and mortar to generate approximately 50 mg of bone powder per sample. DNA extraction followed the procedure described in Dabney *et al.* [33]. These DNA extracts were then converted to single stranded libraries, following the protocol described in Gansauge *et al.*[36], with some modifications[37,38], in the dedicated ancient DNA laboratory at Potsdam University. The protocol included the use of afu uracil-DNA glycosylase (UDG) to remove deoxyuracils at non-terminal base positions resulting from DNA degradation. Each library was barcoded using dual indexing, which included the custom index 2 sequencing primer 'Gesaffelstein'[39] annealing site. The library was quantified prior to sequencing by measuring the DNA fragment size on a Tapestation 2200 (Agilent Technologies) using the D1000 ScreenTape System and the library concentration assessed on a Qubit Fluorometer (ThermoFisher Scientific). Paired-end sequencing (2x50 bp) was carried out on an Illumina HiSeq-2000/2500 v4 high output platform in the Genepool Sequencing Facility at the University of Edinburgh. Each sample was run on 1.5 lanes, generating between 200-300 million reads per sample (Table S1). The European woolly mammoth (Scotland) was additionally processed at the ancient DNA laboratory of Potsdam University. Intact tusk pieces of approximately 200 mg were pulverised in a mixer mill and the resulting powder was divided into five tubes to be used for five separate extractions following the same protocol as above[33]. Each extract was afu UDG-treated and subsequently converted into a single stranded DNA library following the protocol described in Gansauge *et al.*[36]. Each library was barcoded using dual indexing and quantified prior to sequencing by measuring the DNA fragment size on a Tapestation 2200 (Agilent Technologies) using the D1000 ScreenTape System as well as the library concentration on a Qubit Fluorometer (ThermoFisher Scientific). Only four out of five libraries (S1, S2, S3 and S5) showed traces of DNA and were subsequently used for

sequencing. We conducted an initial screening of libraries S1, S2, S3 and S5 at Potsdam University by sequencing approximately 2 million paired-end reads (2x150 bp) on a NextSeq 500 Illumina platform. Further paired-end (2x150 bp) sequencing of approximately 400 million reads for each library was performed at SciLifeLab on the HiSeqX Illumina platform (Table S1).

3. Sequence data processing and mapping

We combined our obtained sequence data with that from previously published[40] elephantid genomes that include all extant and three extinct species (Table S2). For the five samples sequenced here, we trimmed adapters and merged paired-end reads using SeqPrep 1.1[41], initially retaining reads either ≥25 bp (Krestovka, Adycha, Chukochya) or ≥30 bp (Scotland, Kanchalan), and with a minor modification in the source code that allowed us to choose the best base quality score in the merged region instead of aggregating the scores[42]. Three of the ancient genomes in the dataset had been treated with the afu UDG enzyme (the straight-tusked elephant and the Scotland and Kanchalan mammoths, Table S2), which leaves post-mortem DNA damage at the DNA fragment termini. Therefore, for these samples, we removed the first and last two base pairs from all reads before mapping in order to minimize erroneous bases. Next, we mapped the merged reads to a composite reference consisting of the African savannah elephant nuclear genome (LoxAfr4), woolly mammoth mitogenome (Krause mammoth, DQ188829), and the human genome (hg19) using BWA aln v0.7.8 with deactivated seeding (-l 16,500), allowing for more substitutions (-n 0.01) and up to two gaps (-o 2)[43,44]. We used Samtools v0.1.19[45] to process the alignment and filter reads with mapping quality below 30 and we used BEDtools v.2.27.1[46] to split the elephant- and mammoth-mapped regions of autosomes, chromosome X and mitogenomes. Next, we removed PCR duplicates from the alignments using a python script (github.com/pontussk/samremovedup) that takes into account both start and end positions of the reads following Palkopoulou *et al.*[42]. Finally, we removed all reads below 35 base pairs from the BAM-files using samtools to filter out spurious mappings (see Supplementary Section 4).

4. Ancient DNA authenticity and quality assessment

All ancient genomes in this study were UDG treated to reduce biased inferences resulting from post-mortem DNA damage. Given the extreme age of the most ancient samples (Krestovka, Adycha, Chukochya), we extensively assessed the authenticity and quality of our mapped sequence data. First, only reads that mapped uniquely to non-repetitive regions of the LoxAfr4 reference and had a mapping quality ≧30 were retained. To do this, we included the human genome reference (hg19) in our composite reference as a mapping decoy to ensure that reads mapping equally well to conserved genomic regions between LoxAfr4 and hg19 were removed, and thus reducing possible biases caused by human contaminating reads[47]. We next used mapDamage2.0.6[48] to obtain read length distributions for all ancient samples. We observed an uptick in the count of 25-30 bp mapped reads for the two low-coverage samples (Adycha, Krestovka; Extended Data Fig. 3), which is characteristic of spuriously aligned ultrashort reads[49]. To determine sample-specific minimum read length cutoffs, we employed a method to assess the rate of spurious mappings for all reads between 20-35 bp and at 5 bp intervals between 35-50 bp (Fig. S3). In each genome, we sampled all alleles with mapping quality ≥30 and base quality ≥30

at each genomic site and counted how many of these did not match the LoxAfr4 reference. The underlying reasoning is that the rate of allele mismatches should be constant as a function of read length if no spurious alignments are present. It is challenging to accurately map ultrashort reads (e.g. <35 bp)[50], but we expect spurious alignments from short reads (both of endogenous and non-endogenous origin) to have a different rate of mismatches to the reference than correctly-mapped endogenous reads. This allowed us to identify a sample-specific minimum read length cutoff above which we consider reads to be correctly mapped and endogenous (Fig. S3, Table S3). For consistency, we applied the longest sample-specific cutoff (≥35 bp, Krestovka; Fig. S3; Table S3) to all samples in downstream analysis using samtools and awk (samtools view -h filename.bam | 'length($10) > 34 || $1 ~ /^@/' | samtools view -bS - > 35bp.filename.bam). The scripts used to run this analysis are available at (github.com/stefaniehartmann/readLengthCutoff). We present ancient DNA quality statistics for each of the ancient samples in Table S3, for both the sample-specific and 35 bp minimum read length datasets. Based on reads aligned to the LoxAfr4 autosomes, we calculated the (1) count of reads aligned, using the *flagstat* command in SAMtools v.0.1.19[45]; (2) average genomic coverage, using the mean of values derived from *samtools depth -a*; (3) proportion of the genome uncovered, using the count of sites with zero derived from *samtools depth -a* divided by the total length of the autosomes; (4) average read length, using *samtools view -F 4* and bash commands; and (5) deamination frequency at the terminal nucleotide positions, based on the proportion of C>T at the first position in the forward direction as estimated by mapDamage. As all ancient samples were UDG treated, overall cytosine deamination frequencies calculated by mapDamage were low (Table S3). We therefore additionally examined cytosine deamination profiles at CpG sites, which are unaffected by UDG treatment[51], using the *platypus* option in PMDtools (github.com/pontussk/PMDtools)[52]. The three samples processed with afu UDG enzyme during single-strand DNA library preparation (Scotland, Kanchalan, and the straight-tusked elephant) had elevated C>T misincorporations at the terminal positions, as compared to the other ancient samples. For these three samples, we therefore trimmed the first and last two bases from the merged reads, and then remapped and filtered the trimmed reads as outlined above. We show that the average read lengths for the most ancient samples (Krestovka, Adycha, Chukochya) are 42-49 bp, after excluding reads <35 bp (Extended Data Fig. 3; Table S3). These are comparable to other younger specimens, but we note that these younger specimens were either sampled from warmer localities with less optimal DNA preservation (Columbian mammoth, Wyoming woolly mammoth) or processed using laboratory methods (i.e. single-strand DNA library preparation) that generate, and are biased toward the recovery of, ultrashort fragments (Scotland, Kanchalan). However, the Krestovka, Adycha, and Chukochya average read lengths are far shorter than those generated from the Oimyakon (59 bp) and Wrangel (72 bp) mammoths, which are comparable in terms of preservational context (permafrozen) and laboratory processing. The cytosine deamination frequencies at CpG sites are up to three times higher in the Krestovka, Adycha, and Chukochya data sets, as compared to other younger mammoths (Extended Data Fig. 4), which is consistent with their old age.

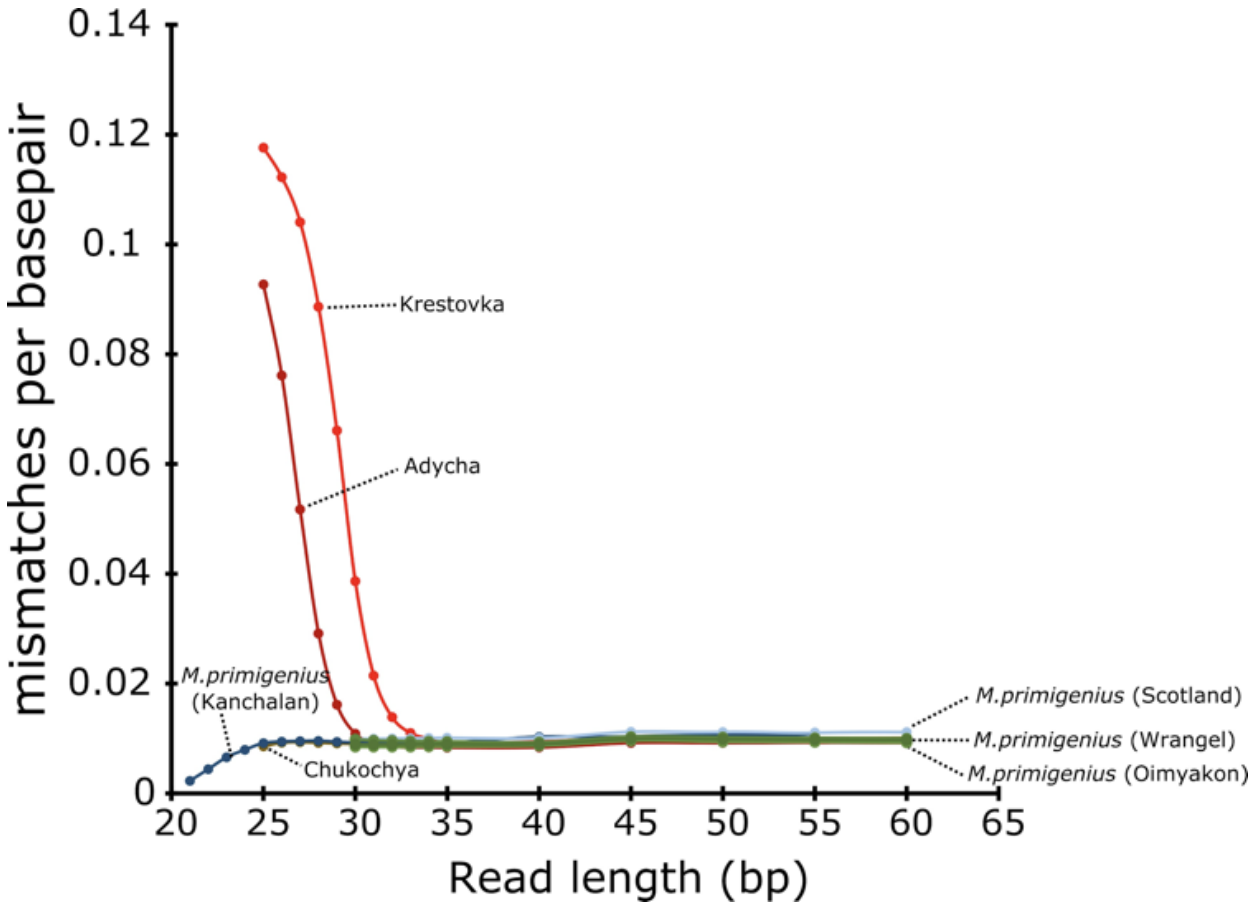

Fig. S3. Average number of mismatches to the reference per base pair across read lengths for all ancient samples. The average number of mismatches per base pair is expected to be constant and independent of read length for endogenous reads. Reads below 30-35 bp in length show elevated numbers of mismatches among the mapped reads, suggesting spurious mappings. Therefore reads <35 bp were excluded from downstream analysis.

5. Reconstruction of mitogenomes, tip-dating, and mtDNA phylogeny

We assembled mitochondrial genomes for the five newly sequenced samples using the iterative, reference-guided assembler MIA[53] and restricting the input reads to those of length ≥35 bp. To identify potential reference bias and alternative convergence outcomes, we created three independent assemblies for each sample, each using a different initial mitochondrial reference with MIA - the African savannah elephant (NC_000934)[40], Asian elephant (NC_005129)[54], and woolly mammoth (NC_007596)[55] - and checked for similarity between these assemblies. For each sample, the three assemblies had 98.9% or greater pairwise identity, with differences falling almost entirely in a repetitive section of the control region. Though each of the three assemblies for each sample were highly similar, to guard against in-group reference bias we chose the assemblies generated with the Asian elephant mitochondrial reference for our subsequent analyses for the three oldest samples (Adycha, Krestovka, and Chukochya). We used the assemblies generated with the woolly mammoth mitochondrial reference for the two Late Pleistocene mammoths from Scotland and Kanchalan. Positions covered fewer than three times or with less than 67% sequence agreement were coded as missing data. This yielded mitochondrial assemblies with coverage of 37.8x, 47.5x, and 77.1x for Adycha, Krestovka, and Chukochya, and 99.6x and 179.5x for the newly sequenced Late Pleistocene woolly mammoth samples from Scotland and Kanchalan (Table S2), respectively. These assemblies were then aligned using Muscle v3.8.31[56], together with previously published (N=166) mammoth[35,57], and *Elephas maximus* (N=2), *Loxodonta cyclotis* (N=6), *Loxodonta africana* (N=3), and *Palaeoloxodon antiquus* (N=4) sequences[58] to create a final alignment containing 187 mitochondrial genomes. The alignment was then separated into six partitions: tRNAs, rRNAs, first, second and third codon positions, and the control region, with a small portion of the control region containing variable numbers of short tandem repeats (VNTR) excluded. For each partition, the best model of molecular evolution was determined using jModelTest v2.1.10[59], based on the Bayesian information criterion (BIC). We identified HKY as the best model for each partition[60] with a gamma-distributed rate heterogeneity[61] and a proportion of invariant sites (HKY+G+I), except for tRNAs, for which the best model was HKY with a proportion of invariant sites (HKY+I). To estimate the age of the three oldest *Mammuthus* samples (Adycha, Krestovka, Chukochya), we performed a Bayesian reconstruction of the phylogenetic tree using BEAST v1.10.4[62], calibrating the molecular clock using tip ages for all ancient samples with a finite radiocarbon date, as well as a lognormal prior on the divergence of *Loxodonta* and *Elephas/Mammuthus* of 5.3 Ma [40]. We compared two priors: a 5.3 Ma divergence, derived from nuclear genomic analyses of the divergence between *Loxodonta* and *Mammuthus*[40], and a 7.6 Ma divergence, derived from a previous mitogenome-based estimate that is consistent with the fossil record[54]. For both priors, we used a standard deviation of 500,000 years. The discrepancy between these calibration points is likely caused by ongoing gene flow among elephantids after morphological diversification, and therefore the two calibrations encompass the range of plausible ages for the divergence of *Loxodonta* and *Mammuthus* mitochondrial lineages. We assumed a strict molecular clock and the flexible skygrid coalescent model[63] to account for the complex cross-generic demographic history of the included taxa; however, model comparison with marginal likelihoods did not favor either the skygrid or a constant population size coalescent model. The ages of all undated ancient samples

or those with non-finite radiocarbon dates were estimated by sampling from log-normal distributions with priors based on stratigraphic context and previous genetic studies (Table S4). We ran two MCMC chains of 100 million generations, sampling every 10,000 and discarding the first 10% as burn-in. Convergence of each chain was assessed using Tracer v1.7.1[64] and chains were then merged using LogCombiner. The maximum clade credibility tree was identified using TreeAnnotator and visualized in FigTree v1.4.4. Because of the possibility of back mutations in the faster-evolving control region, we additionally repeated each analysis excluding the control region (Table S5). The specimen age measurements for the full mitochondrial genome based on the 5.3 Ma prior yielded estimates of 1.65 Ma (95% HPD: 2.08-1.25 Ma), 1.34 Ma (1.69-1.06 Ma), and 0.87 Ma (1.07-0.68 Ma) for Krestovka, Adycha and Chukochya, respectively (Fig. 1). Using a 7.6 Ma root prior provided specimen age estimates of 2.32 Ma (95% HPD: 2.83-1.21 Ma), 1.88 Ma (2.25-1.53 Ma) and 1.21 Ma (1.45-0.99 Ma), respectively (Fig. S4). Age estimates obtained excluding the control region were 1.80 Ma (2.24-1.41 Ma), 1.41 Ma (1.77-1.09 Ma), and 0.87 Ma (1.06-0.69 Ma) for Krestovka, Adycha and Chukochya, respectively, using the 5.3 Ma root prior, and 2.59 Ma (3.10-2.09 Ma), 2.01 Ma (2.43-1.62 Ma), and 1.23 Ma (1.45-1.00 Ma) using the 7.6 Ma prior (Table S5). The root calibration of 7.6 Ma, representing a mitogenome-based estimate of the divergence between African elephant and mammoth that is more consistent with the fossil record[54], provided specimen age estimates that were considerably older and in some cases exceeded the plausible upper age limits obtained from biostratigraphic and palaeomagnetic data. We note that accurately estimating sample ages based on mtDNA is challenging due to the possibility of gene flow among lineages that may have impacted sorting of the mitogenome lineages as well as the reliance on accurate priors for calibration[57].

6. Genetic age estimates based on autosomal data

To obtain additional support for the age estimates of Adycha and Chukochya (Krestovka was excluded as too few autosomal bases are available for this analysis), we calculated specimen ages based on the autosomal data following the method described in Meyer *et al.*[65]. To do this, we counted the number of derived changes in each *Mammuthus* genome since the common ancestor of *Mammuthus* and the African savannah elephant, using the American mastodon (*M. americanum*), and African savannah and Asian elephant genomes as outgroups. Since derived variants accumulate over time, a smaller number of derived changes indicates a shorter lineage, i.e. an older age for the sample material, under the assumption of a strict molecular clock on all lineages. We inferred the ancestral state for a given base in the African elephant reference genome by requiring that the alignments of the mastodon, two African elephants and five Asian elephants are present and identical at that nucleotide. In order to arrive at a date estimate, we used the high coverage Wrangel mammoth, radiocarbon dated to ~4,300 calendar years old, as a calibration point[42]. Each difference to the ancestral state was then counted for the Wrangel genome and the focal *Mammuthus* genome for which both genomes had a called genotype. With the number of derived changes in the Wrangel genome, nW, and the derived changes in the other *Mammuthus* genome, nM, we calculate the relative age of each individual as (nW – nM)/nW, and arrive at an estimate in years by multiplying this quantity with an assumed divergence time to the common ancestor of African elephant and woolly mammoth of 5.3 million years[40]. We note that

this divergence time corresponds to an estimated mutation rate of 0.58×10^{-9} per base pair per year. However, we caution that the elephantid mutation rate is highly uncertain[40,42] and when more accurate estimates become available in the future all absolute time estimates should be rescaled. Finally, in order to compute the variance in the dating estimates, we calculated the branch shortening in windows of 5 Mb and computed bootstrap confidence intervals as 1.96× standard error around the date estimates.

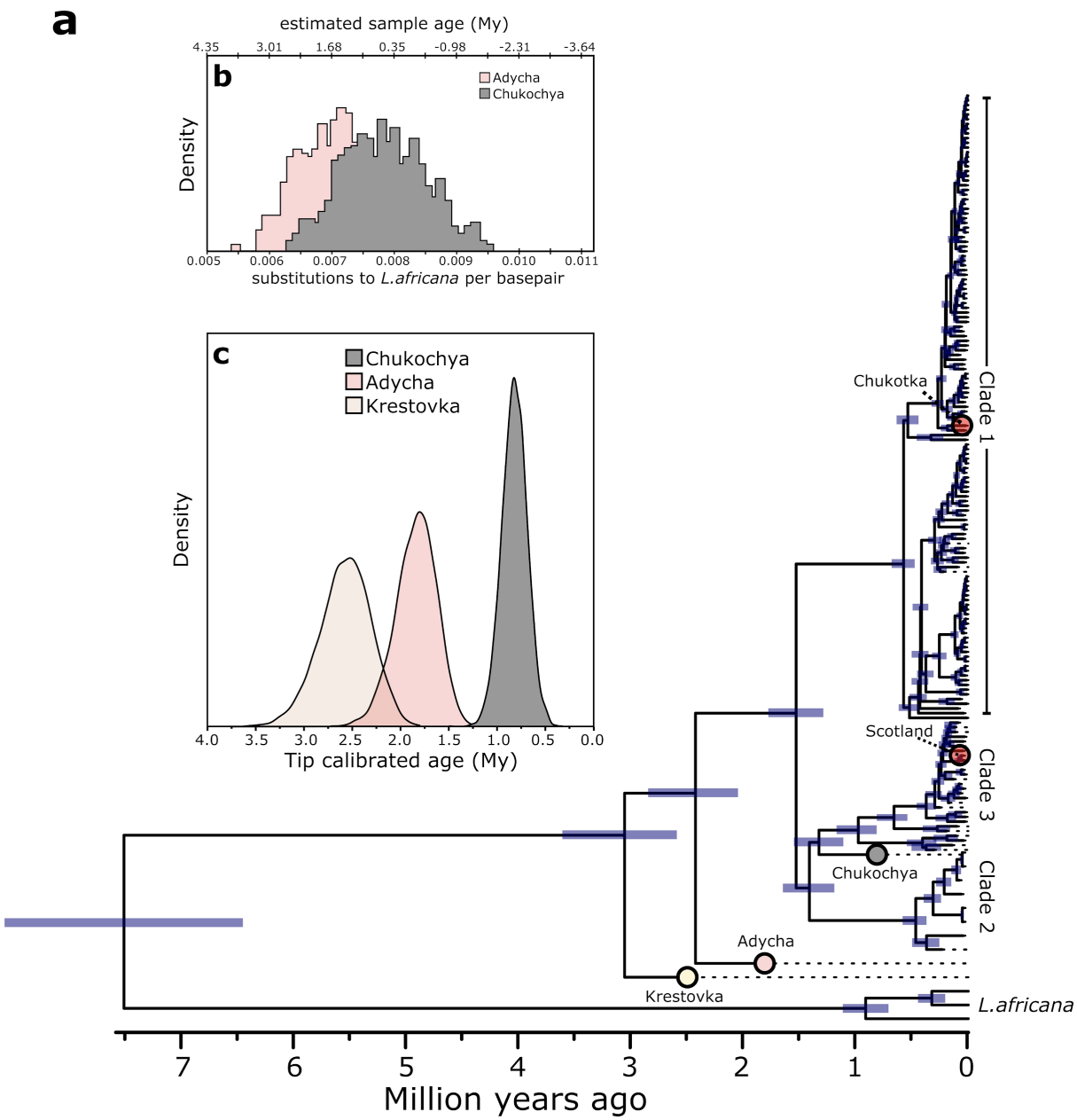

Fig. S4. (a) Bayesian reconstruction of the mitochondrial tree, calibrating the molecular clock using the radiocarbon dates of ancient samples for which a finite radiocarbon date was available, as well as assuming a log-normal prior on the divergence between the African savannah elephant (*L. africana*) and mammoths with a mean of 7.6 million years. Blue bars reflect 95% HPD. Circles depict the position of the newly sequenced genomes. **(b)** Densities for age estimates of samples Adycha and Chukochya based on autosomal data assuming a divergence between the African elephant and mammoths of 7.6 million years. **(c)** Densities for age estimates of samples Krestovka, Adycha and Chukochya based on the mitochondrial Bayesian reconstruction assuming a divergence between the African elephant and mammoths of 7.6 million years.

7. Nuclear genetic relationships and phylogeny

To assess the genetic relationship between the samples, we constructed phylogenetic trees based on the whole genome Identical-By-State (IBS) matrix for all the individuals, excluding sex-chromosomes, with the "doIBS" function in ANGSD. As the European mammoth genome contained some elevated post-mortem DNA damage we excluded transitions. We then calculated pairwise genetic distances between individuals using the full dataset, as well as 100 bootstrap replicates based on 100,000 sites each. Finally, we obtained the phylogenetic tree using a balanced minimum evolution (ME) method as implemented in FASTME[66]. We ran the same phylogenetic method for either all sites, but excluding the Scotland mammoth due to slightly elevated levels of remaining post-mortem DNA damage (Fig. S5a), or transversions only (Fig. 1b, S5b). We then inferred population divergence times using the obtained phylogeny and running a relative-time maximum likelihood clock using the Tamura-Nei model in MEGAX[67], calibrating the tree on a log-normal distributed divergence time between *L. africana* and *E. maximus* of 5.3 ± 0.5 million years (Fig. S6). Next, we inferred relative population split times using an approach that examines single nucleotide polymorphic (SNP) positions that are heterozygous in an individual from one population and measures the fraction of these sites at which a randomly sampled chromosome from an individual of a second population carries the derived allele, polarized by an outgroup (F(AlB)) statistics[50]. The lower this fraction the more drift has occurred between the compared genomes, and thus the older their genetic divergence. The fraction is expected to be around 1/3 for an individual from the same population, and 0 in an individual from a distantly related population, since novel mutations accumulate in each population after their split. We ascertained heterozygous sites in three high-coverage genomes — *E. maximus* and *M. primigenius* (Oimyakon and Wrangel)[42] — using the SAMtools v.0.1.19[45] 'mpileup' command, bcftools, and the 'vcf2fq' command from vcfutils.pl. We only included SNPs with a quality ≥30 and within non-repetitive regions. Additionally we filtered sites below 1/3 or above two times the genome-wide average coverage, and excluded calls at CpG-sites and within 5 bp of indels. For each of the *Mammuthus* genomes, we then estimated the proportion of sites for which a randomly drawn allele at the ascertained heterozygous sites matches the derived state.

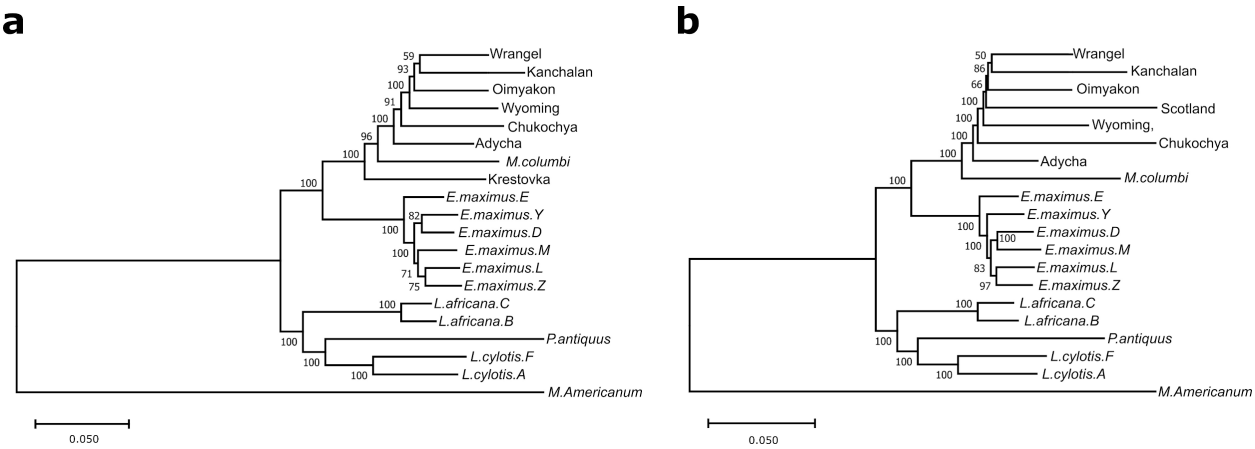

Fig. S5. Minimal evolution phylogenies based on **(a)** all sites autosomal sites, excluding the European mammoth (Scotland) due to elevated levels of C>T substitutions, and **(b)** all autosomal transversions, excluding Krestovka due to limited data.

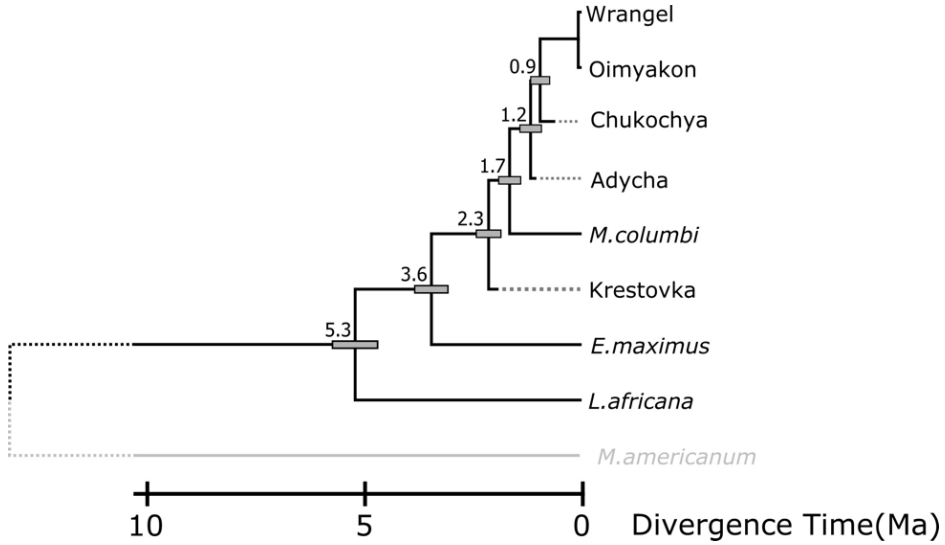

Fig. S6. Relative-time maximum likelihood calibrated tree assuming a normal distribution divergence between the African savannah elephant (*L. africana*) and Wrangel Island mammoth of 5.3 ±0.5 million years.

8. D, f4-statistics, AdmixtureGraphs and TreeMix

We tested for evidence of admixture between elephantid lineages by computing D-statistics and f_4-statistics, which count the occurrences of shared alleles between genomes. Asymmetrical allele sharing between lineages with respect to the genetic phylogeny can indicate episodes of gene-flow after the split between the tested populations[50]. Although these statistics were originally developed for genomes relatively contemporary to each other[50], it has since become clear that the same statistics can be applied for the analysis of genomes separated in time. Despite these statistics not having been applied before to samples separated by over 1 million years, as in this study, the application of these population genetic methods to processes unfolding at these timescales is not new or unusual. From the perspective of methods that exploit shared genetic drift, (e.g. D- and f-statistics, admixturegraphs, and TreeMix), it is not the age of the genomes themselves, but the time depth of population divergence and subsequent genetic drift that is modelled[68]. Independent of whether genomes split into separate populations or go extinct, the consequence for these methods is essentially the same: genetic drift stops being correlated between these genomes. New private mutations on the surviving branch after the death of (or divergence from) the other genome will not affect how much drift they share since only shared derived mutations are considered in the statistics and subsequent models. Once a population divergence becomes sufficiently old, there will be no shared variation between the descendant populations for these methods to exploit. However, mammoths and elephants have evidently not yet reached that point, and there is enough shared variation for these methods to obtain confident inferences. This can be understood by the expected time of 4Ne generations from mutation to fixation only being an average[69], with the majority of new mutations ($1-(1/4N_e)$) indeed never reaching fixation before becoming extinct. As Kimura and Ohta (1973) noted, many mutations are old, such that for example "*a neutral mutant whose current frequency is 10% has the expected age roughly equal to the effective population size Ne and the standard deviation $1.4N_e$ (in generations)*". Assuming a effective population size of ~13,000 in the relevant period and a generation time of 31 years[42], the average age of a 10% frequency mutation would be 2x13,000*31=806,000 years, but with a standard deviation of 1,140,000 years, such that ~15% of those mutations would have an age of more than 1,940,000 years. It is thus not surprising to find shared polymorphism between these ancient genomes. We have now added a section in Supplementary Information Section 8 explaining this. It is thus not surprising to find shared polymorphism between these ancient genomes. Indeed, many successful applications of drift-based methods have been applied to study relationships and admixture involving populations where divergences occurred on the time scales of millions of years, including modern and archaic humans (divergences ~0.7-1 Ma, equivalent to ~1.4-2 Ma evolutionary distances when considering both branches)[70], and brown, polar and cave bears (divergences >1 Ma, and with considerably faster generation times)[71]. The same methods have also previously been applied to elephants and mammoths, including straight-tusked elephants that are even more diverged from recent mammoths (>5 Ma) than the genomes we analyse here[40].

The f_4-statistics and admixture graph framework explicitly track genetic drift, and therefore assume that variants are polymorphic in the common ancestor of the analysed populations.

Ascertainment of variants in an outgroup population is the preferred approach to meet this criterion in empirical data[68]. We thus used Admixtools to calculate D and f_2,f_3,f_4-statistics for all possible quadruple combinations of samples iterating through the four different groups (H1, H2, H3, and outgroup) based on randomly sampled alleles, conditioning on all sites that are polymorphic among the six Asian elephant genomes (n = 9,892,076) (Table S6)[68]. The mastodon (*M. americanum*) was used as the outgroup in all comparisons . Since our genomes are UDG treated we do not expect differences in D- and f-statistics calculated on all sites or only transversions. Indeed the obtained values were nearly identical (Fig. S7) and we subsequently used the obtained values when including all SNPs. The D-statistics analysis revealed significant excess allele sharing between Krestovka and the Columbian mammoth, as well as between the Columbian mammoth and a North American woolly mammoth from Wyoming (Fig. 2a). For all other comparisons, the D-statistics were non-significant, which is consistent with the Adycha and Chukochya genomes being ancestral to all Late Pleistocene woolly mammoths. Interestingly, all mammoths, including Krestovka, shared an equal number of derived alleles with the straight-tusked elephant (Fig. 2a). This suggests that the gene flow between mammoths and the ancestors of the straight-tusked elephant identified in Palkopoulou *et al.*[40] took place before the Krestovka genome diverged from the other mammoth genomes, i.e. prior to 1.2 Ma before present based on the stratigraphic age of the Krestovka specimen and potentially much earlier (>1.8 Ma) based on our genomic divergence estimates. Consequently, our analyses imply that this introgression must have taken place in Africa, before straight-tusked elephants expanded into Eurasia at c. 0.8 Ma[72]. Next we used the admixturegraph R package[73] to assess the genetic relationship among *Mammuthus* genomes using admixture graph models, fitting graphs to all possible f_4-statistics involving a given set of genomes. To resolve the relationships of the Adycha, Krestovka, and Chukochya samples within the population history of mammoths, we exhaustively tested all 135,285 possible admixture graphs (with up to two admixture events) relating these three individuals, one woolly mammoth (Wrangel), one Columbian mammoth, and one Asian elephant, setting the latter as outgroup. All graph combinations in which the Asian elephant would be modelled as the product of admixture, and thus could not be set as a correct outgroup, were ignored. We evaluated all remaining graphs using f_4-statistics calculated only on variants ascertained at polymorphic sites among the six Asian elephant genomes, thereby ensuring that the statistics reflect genetic drift at sites that were polymorphic in the mammoth ancestral population, to account for the temporal time-span of our samples[68]. For each graph, the best scoring fit, as assessed using the "best_error" score calculated by the admixturegraph package, from five independent iterations was retained (Fig. 2b, Fig. S8). We also constructed admixture graphs using the above described f_4-statistic with qpBrute[74], a brute-force implementation of the qpGraph AdmixTools software[68]. qpBrute runs a stepwise addition algorithm to add new leaf nodes to the graph. At each step, insertion of a new node is tested at all branches of the graph, except the outgroup branch (*E. maximus*). Where a node can not be inserted without producing f_4 outliers (i.e. |Z| >=3) all possible admixture combinations are also attempted. In addition, the f_2- and f_3-statistics are used to estimate shared genetic drift and branch lengths. The resulting list of all fitted graphs was then passed to the MCMC algorithm implemented in the admixturegraph R package, to compute the marginal likelihood of the models and their Bayes Factors (BF). The

most parsimonious model (the fewest admixture events) with the highest fit to the data is shown in Extended Data Fig. 6.

The signal of additional shared ancestry between the Columbian mammoth and the woolly mammoth from Wyoming, as inferred from the D-statistics, suggests a second admixture pulse (Fig. 2). Using AdmixTools, we inferred the ancestry proportions with an f_4-ratio test[68]. This is a ratio of two f_4-statistics (alpha = f_4 (A, O; X, C)/ f_4(A, O; B, C)) where X represents the admixed population, B and C the source populations or two populations related to the sources, A a population related to source population B, and O an outgroup. We set the woolly mammoth from Wyoming as the admixed individual (X), the Oimyakon woolly mammoth as source B, Columbian mammoth as source C, the Wrangel woolly mammoth as the individual related to the woolly mammoth source (A), and the mastodon as outgroup. We inferred the proportion of shared ancestry between the Columbian Mammoth and Wyoming woolly mammoth as 10.7% – 12.7% (95% confidence interval). In addition, we estimated genetic relationships and admixture among the *Mammuthus* samples by constructing a maximum-likelihood tree with migration edges using TreeMix v.1.12[75]. We first estimated the allele frequencies from the randomly sampled alleles (note that the allele frequencies reflect either 0 or 2 ancestral alleles for each genomic site), and then ran the TreeMix model accounting for linkage disequilibrium (LD) by grouping sites in blocks of 1,000 SNPs (-k 1,000) setting the Asian elephant (*E. maximus*) samples as root. Standard errors (-SE) and bootstrap replicates (-bootstrap) were used to evaluate the confidence in the inferred tree topology. After constructing a maximum-likelihood tree, migration events were added (–*m*) and iterated 10 times for each value of *m* (1–10) to check for convergence in the likelihood of the model as well as the explained variance following each addition of a migration event (Fig. S9). The inferred maximum-likelihood trees were visualized with the in-built TreeMix R script plotting functions (Fig. S10).

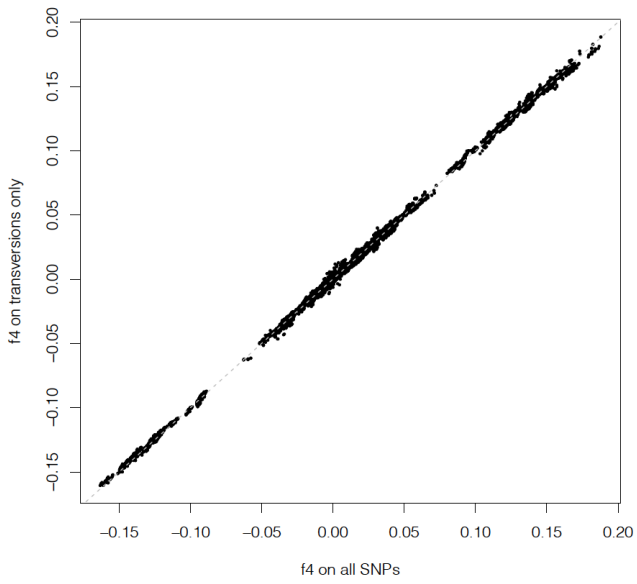

Fig. S7. Correlation between f_4-statistics calculated on all SNPs and only transversions.

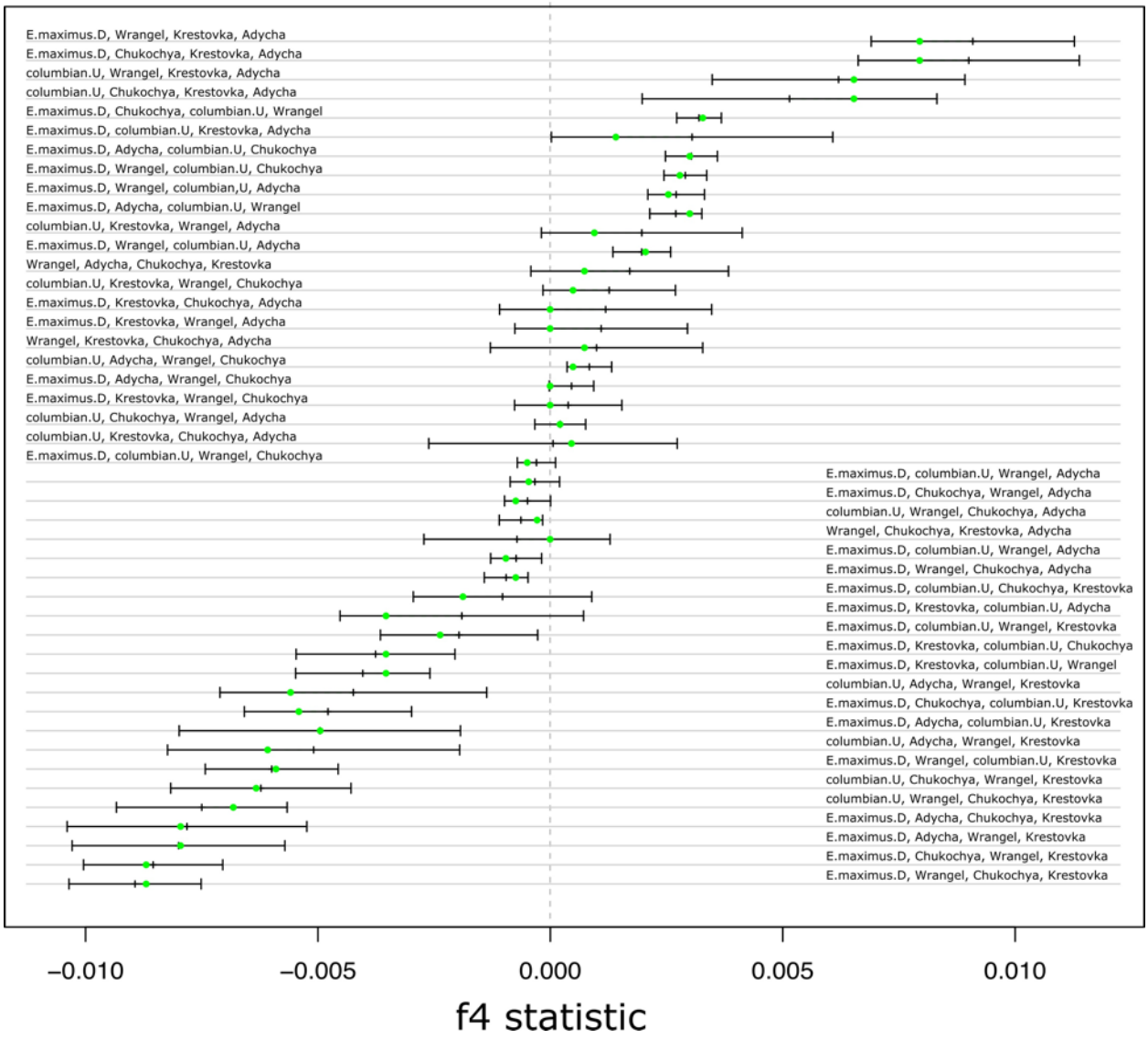

Fig. S8. Observed (black error bars) versus predicted (green points) f_4-statistics for the best fitting admixture graph model with one admixture event. Black error bars depict ± 3 standard errors around the observed f_4-statistics. All f_4-statistics (n = 45 pairwise combinations) fit within the model without outliers.

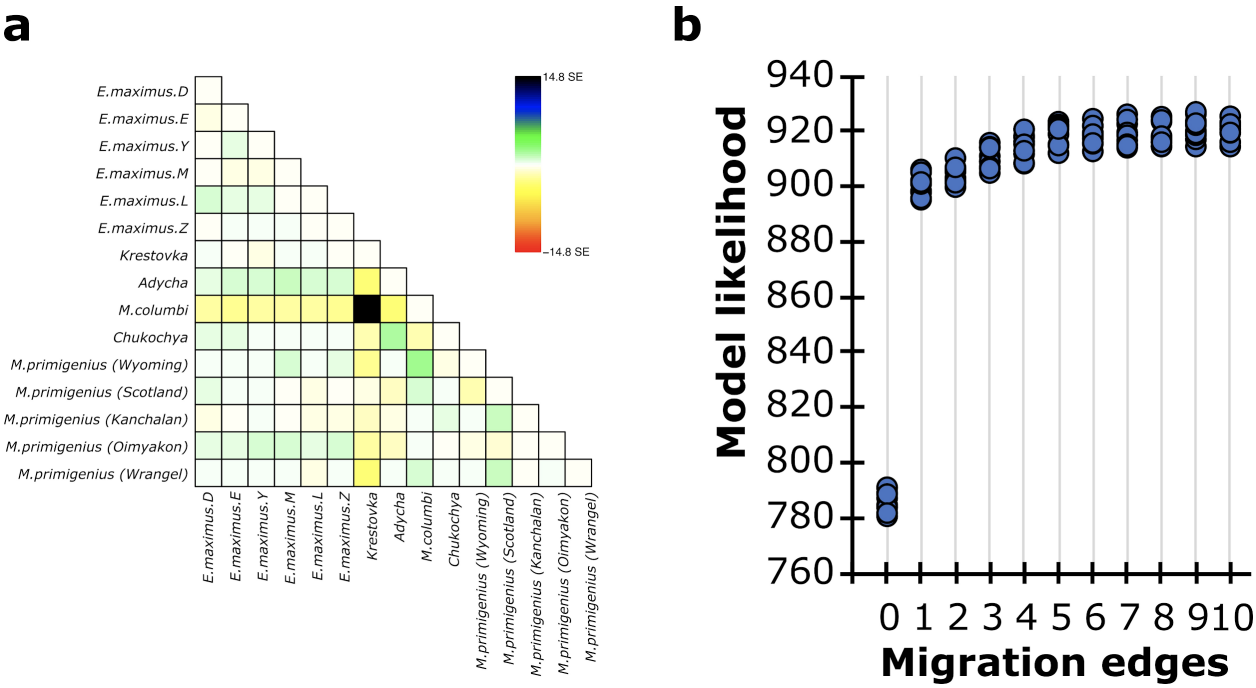

Fig. S9. (a), shows residuals for the treemix model with no migration events and **(b)**, shows obtained likelihood values for each of the models for 0 to 10 migration edges.

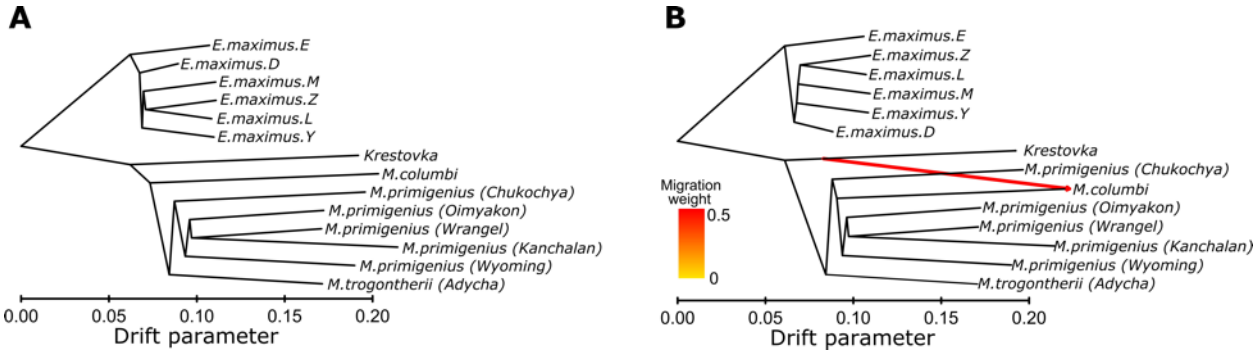

Fig. S10. Maximum-likelihood phylogenies as obtained from TreeMix with **(a)** no admixture events and **(b)** one migration event. Note the placement of the Columbian mammoth (*M. columbi*), which in panel A falls outside the woolly mammoth (*M. primigenius*) clade whereas in panel B the Columbian mammoth falls inside the woolly mammoth diversity with a strong admixture edge (41%) from the Krestovka lineage.

9. Ghost admixture in Columbian and European mammoths

To further test for admixture, we used a hidden Markov model that does not require any genomic information from the admixture source[76]. This method identifies genomic regions within a given individual that likely came from admixture with a distant lineage not present in the dataset based on the distribution of private sites (i.e. ghost admixture). This analysis was done for the Columbian mammoth, to further investigate the admixture identified in the analyses described above. In addition, we also included the 45 ka old European mammoth genome (Scotland) in this analysis. The rationale for this latter analysis was that, based on dental morphology, Lister *et al.*[3,32] proposed that although Late Pleistocene European mammoths were derived from woolly mammoths dispersing from Siberia, late-surviving steppe mammoths (*M. trogontherii*) in Europe may have contributed to their ancestry. We estimated the number of callable sites, the SNP density (as a proxy for per-window mutation rate) and the number of private variants with respect to a set of outgroup elephant genomes in 1 kb windows. We applied settings for zero or one gene flow event. Starting probabilities were set to (0.6, 0.4) and (0.95, 0.05) for the Columbian and Scotland mammoth respectively to reflect the previous ancestry percentage estimates, but we note this method is relatively robust to initial starting priors[76]. The transition matrices were set to (0.999, 0.001),(0.012, 0.98)). We then tested for ghost admixture in the Columbian mammoth, using sites private to the Columbian mammoth with respect to all other genomes in this study except Krestovka (Fig. S11). For the European mammoth, we only counted private alleles as those not present in any of the other individuals in this study (Fig. S11). The decoding was performed as provided by the package (github.com/LauritsSkov/Introgression-detection/), at a probability cutoff of 0.9 and with a minimum number of 5 private sites per region to call introgressed fragments. In the Columbian mammoth 41% of the windows were identified as originating from a ghost lineage with such genomic regions distinct from the *M. primigenius* (Extended data Fig. 7). In contrast, when forcing ghost admixture into the model for the European mammoth the best fitting was observed for a scenario of 46% ghost admixture of a lineage highly similar to M. primigenius (Fig. S12). The absence of clearly distinct genomic components in the European mammoth suggests that no significant ghost admixture from a genetically divergent lineage into this mammoth occured. We obtained fasta-alignments for the autosomal regions in the Columbian mammoth's genome identified as "un-admixed" and "ghost-admixed" regions by calling a random base at each covered position using ANGSD. Minimal evolution phylogenies were then obtained for both alignments as in Supplementary Section 8. Those genomic regions identified as being a result of ghost admixture in the Columbian mammoth are most closely related to the Krestovka mammoth, whereas the un-admixed regions of the genome fall within the woolly mammoth diversity (Fig. S12). Finally, for the Columbian mammoth genome and in 100 kb windows, we counted the number of pairwise differences to the Wrangel woolly mammoth genome and Krestovka genome for those sites that have an allele call in all three genomes. An estimated 39% of the windows in the Columbian mammoth genome are closer to Krestovka than to the Wrangel (*M. primigenius*) genome. A small fraction of the Oimyakon woolly mammoth genome (~0.2%) is also closer to the Krestovka genome than to the Wrangel genome, possibly as a result of incomplete lineage sorting and/or false positive inferences (Fig. S13).

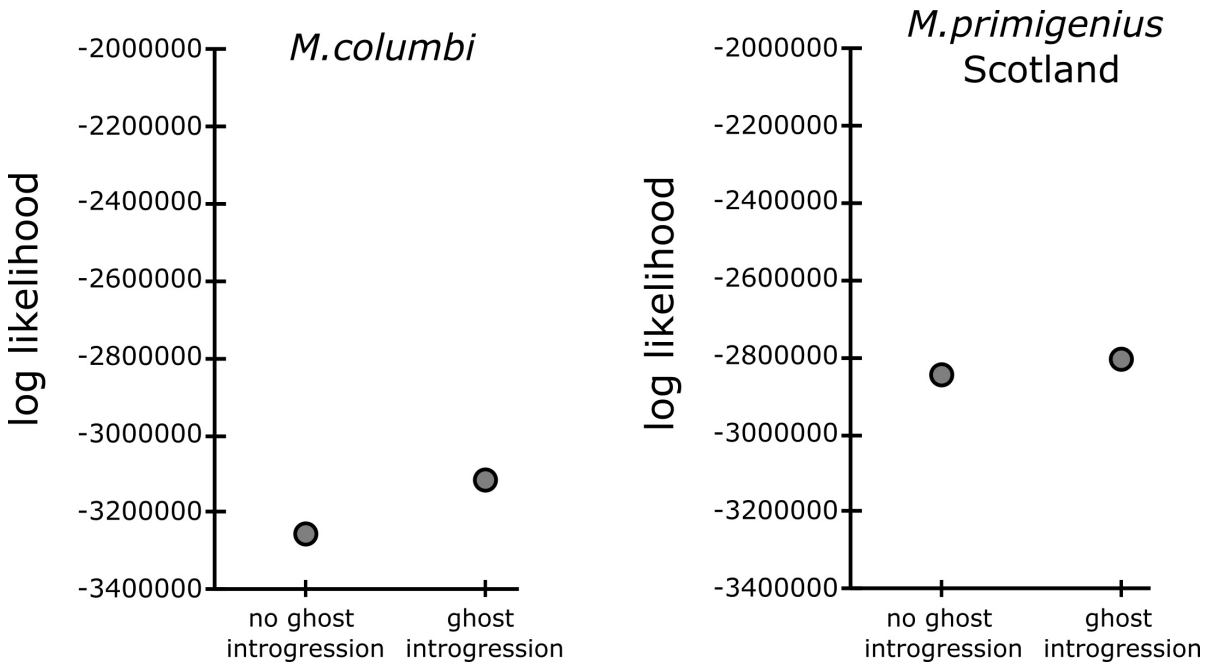

Fig. S11. Model-likelihood values without or with ghost introgression. Adding ghost introgression to the Columbian mammoth resulted in higher model fit to the observed data, whereas in the European woolly mammoth (Scotland) no such increased model fit was observed when adding ghost-admixture.

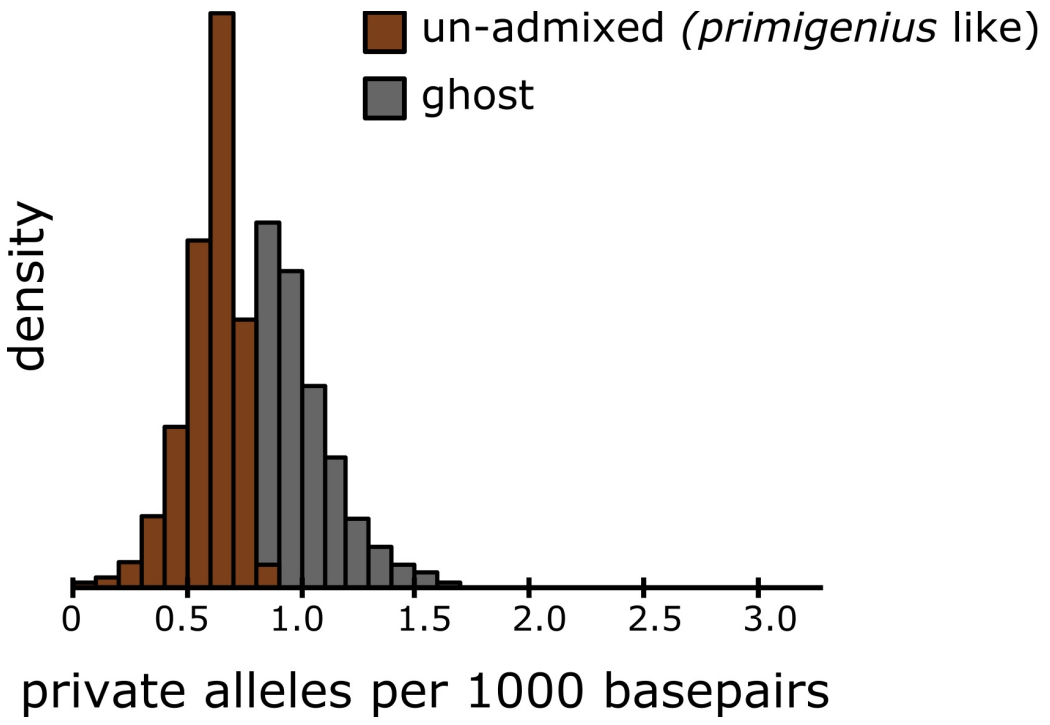

Fig. S12. The number of private alleles per 1000 bp within genomic regions identified as woolly mammoth (*M. primigenius*) or ghost ancestry for the Scotland mammoth genome.

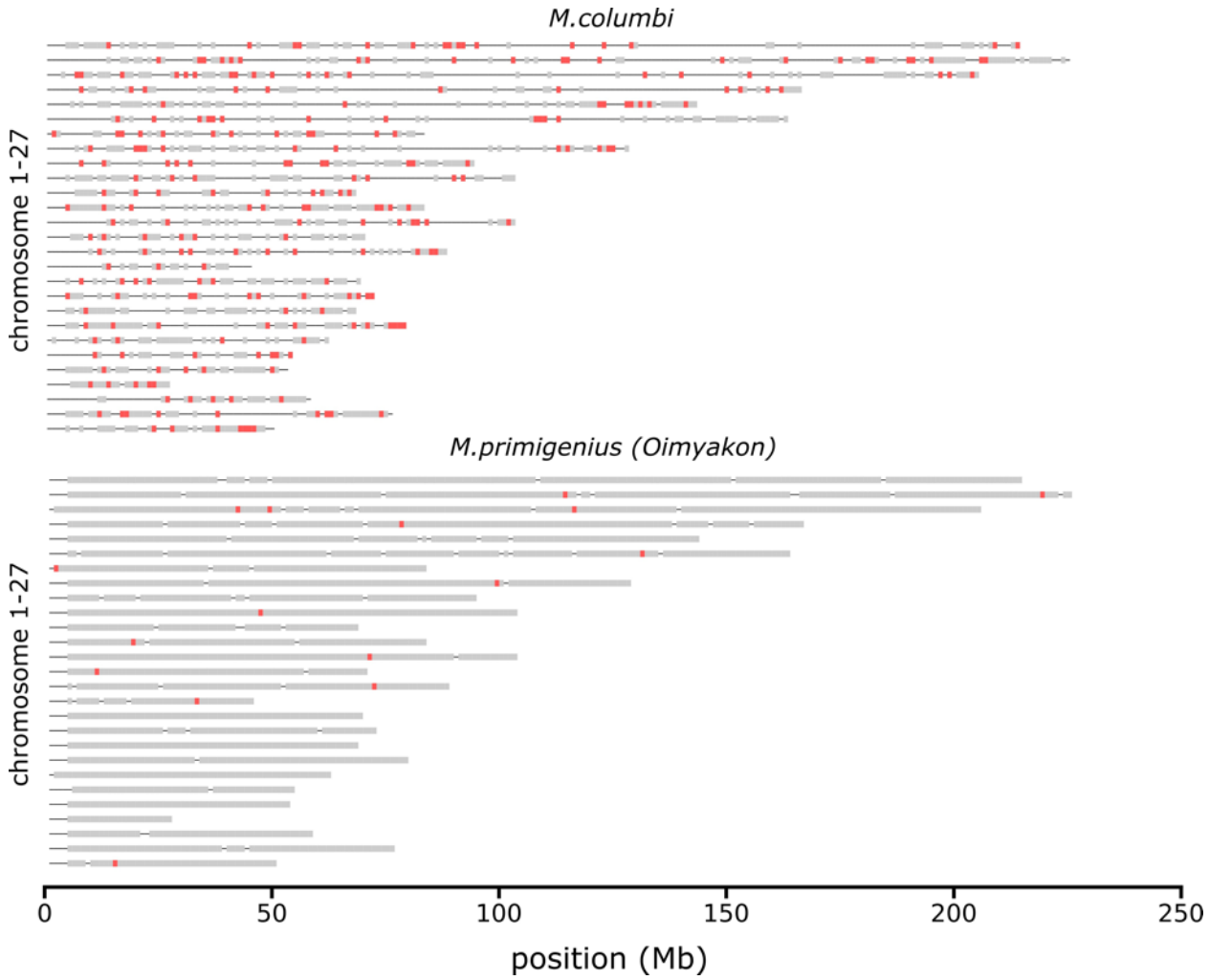

Fig. S13. A map of putative Krestovka ancestry in the Columbian mammoth (*M. columbi*) genome and Oimyakon woolly mammoth (*M. primigenius*) genome, which was used as a control. Red windows depict those closest to the Krestovka genome and grey regions are closest to the Wrangel (*M. primigenius*) genome. Thin lines depict genomic regions with missing data.

10. Genetic adaptations of the woolly mammoth

Our deep temporal sampling allowed us to estimate the timing of genetic adaptations in the woolly mammoth lineage. To investigate this, we built a chain file to lift over our sampled allele dataset to the annotated LoxAfr3 reference genome by aligning the LoxAfr3 and LoxAfr4 references using *last*[77]. First, a reference index was made using *lastdb (*-P0 -uNEAR -R01). We then aligned the two references using *lastal* (-m50 -E0.05 -C2). The alignment was converted to MAF format (*last-split -m1)* and finally to a chain file with the *maf-convert* tool (last.cbrc.jp). The Picard Liftover tool ('Picard Toolkit', 2019) together with the obtained chain-file was then used to lift over the identified variants to the LoxAfr3 reference. Using the African savannah elephant genome annotation (LoxAfr3.gff), we identified all amino-acid changes where all Late Pleistocene woolly mammoth genomes carry the derived state and all other elephantid genomes carry the ancestral allele with VariantEffectPredictor[78]. Next, for each of these amino-acid changes, we assessed the state (derived or ancestral) among the three oldest samples (Krestovka, Adycha, Chukochya) and the Columbian mammoth (Table S8). The state (ancestral or derived) for a set of genes likely involved in Late Pleistocene woolly mammoth specific adaptations as identified in Fry *et al.*[79] and Lynch *et al.*[80] is listed in Table S10. Finally we ran a Gene Ontology enrichment on all genes for which the woolly mammoth, and Adycha and Chukochya genomes are derived and all other elephantid genomes ancestral using GOrilla[81] (Fig. S14).

Next, we scanned for positive selection signatures in coding regions in the Late Pleistocene woolly mammoth genomes using PAML[82]. Using the African savannah elephant genome annotation we generated consensus coding sequences for *Loxodonta* species (*L. africana* and *L. cyclotis*), *E. maximus*, *Mammuthus primigenius* and *Mammut americanum*. We masked positions showing within-species polymorphism, and further removed any coding sequences containing indels, where the coding sequence length was not a multiple of three, contained premature stop codons or lacked a stop codon, resulting in 6,808 genes. In addition, we created a second dataset that included gene sequences from two outgroup species from the most closely related orders for which a genome is available, *Procavia capensis* (hyrax) and *Echinops telfairi* (lesser hedgehog tenrec). We downloaded gene sequences of these two species from Ensembl Biomart v98[83], chose one-to-one orthologs with the African elephant genes as determined by Ensembl Compara, and aligned these with the elephantid consensus sequences using MUSCLE[56] resulting in a second dataset with 1,746 genes. Multiple sequence alignments of both datasets were analysed using the branch-site model of PAML's "codeml" algorithm[82], comparing a model that allows for positive selection on the mammoth branch (foreground) vs. the null model of relaxation of constraints across the phylogeny, for each gene (Model=2, NsSites=2, omega=1, using fix_omega = 0 or fix_omega = 1 for the positive selection or null models, respectively). The branch lengths in the phylogeny were derived from TimeTree[84]. In total, four genes in the first dataset and one gene in the second dataset showed nominally significant differences between the two branch-site models at nominal p-value<0.05 (likelihood ratio test, chi-square df=1) and also contained at least one codon site identified to be under positive selection using codeml's Bayes empirical Bayes procedure (posterior p>0.95), *i.e.* changes specific to the *M. primigenius* lineage (no gene was identified as significant after multiple testing correction). Finally, we compared the genotypes of the three oldest samples (Krestovka, Adycha, Chukochya) and the Columbian

mammoth at the mammoth-specific codon changes (n=11) found across these five genes (Table S11).

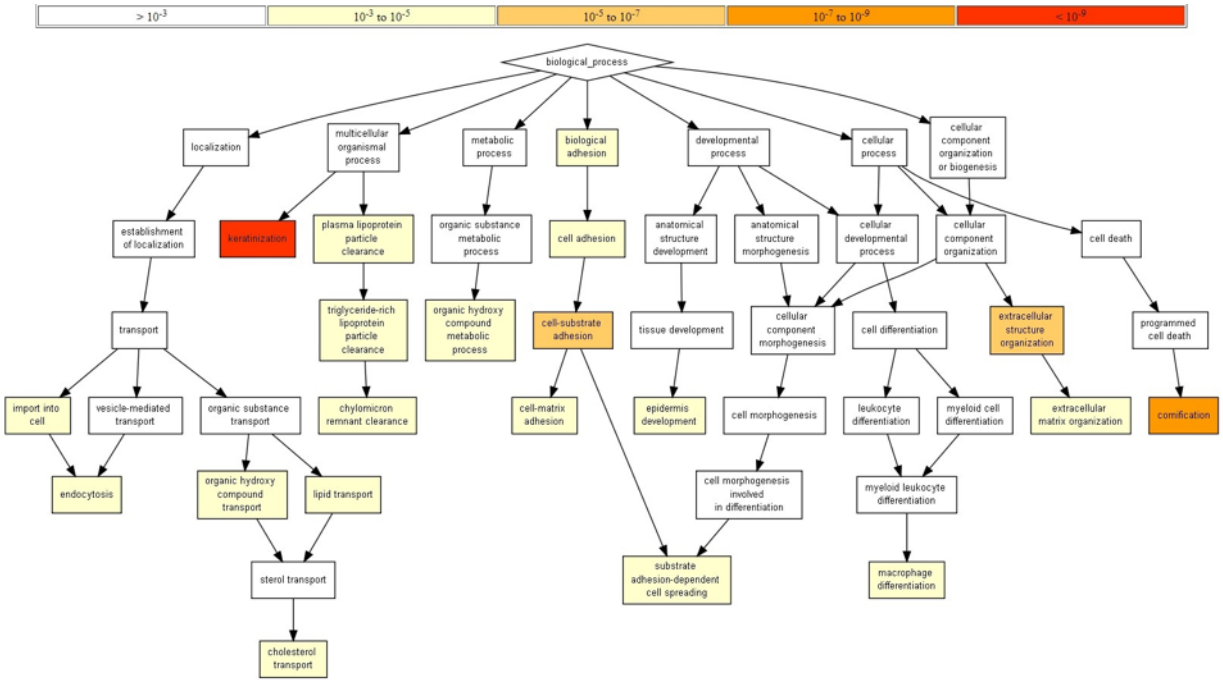

Fig. S14. Gene Ontology enrichment on all genes for which the Asian and African elephants have the ancestral allele, and all woolly mammoths (including Chukochya) and the *trogontherii*-like mammoth (Adycha) have the derived allele.

References

1. Sher, A. V. On the history of mammal fauna of Beringida. *Quartärpaläontologie* **6**, 185–193 (1986).
2. Lister, A. M. & Sher, A. V. The origin and evolution of the woolly mammoth. *Science* **294**, 1094–1097 (2001).
3. Lister, A. M. & Sher, A. V. Evolution and dispersal of mammoths across the Northern Hemisphere. *Science* **350**, 805–809 (2015).
4. Sher, A. V. *et al.* Late Cenozoic of the Kolyma Lowland: XIV Pacific Science Congress, Tour Guide XI, Khabarovsk August 1979. Moscow, Academy of Sciences of the USSR, 1-116. in *XIV Pacific Science Congress, Moscow [in Russian and English]* (1979).
5. Sher, A. V. Age of quaternary deposits of the Iana-Kolyma lowland and its mountainous framing. *Dokl. Akad. Nauk SSSR* **278**, 708–713 (1984).
6. Churcher, C. S. A mammoth measure of time: Molar compression in Mammuthus from the Old Crow Basin, Yukon Territory, Canada. *Curr. Res. Pleist* **3**, 61–64 (1986).
7. Sher A.V., Kaplina T.N., Ovander M.G. Arkhangelov A.A., Bashlavin D.K., Tomirdiaro S.V., Gilichinsky D.A. Sulerzhitsky L.D. Resolution of Interdepartment Stratigraphic Conference on the Quaternary System of the USSR (Magadan, 1982). Explanatory Notes to the regional stratigraphic charts of the Quaternary deposits. *Magadan* 241 (1987).
8. Zazhigin, V. S. Early evolutionary stages of collared lemmings (Dicrostonychini, Microtina, Rodentia) as characteristic representatives of Beringian subarctic fauna. *Beringia in Caenozoic Era. Kontrimavichus V.L. (Ed.). USSR AS, Far-Eastern Scientific Center.* **280-288**, (1976).
9. Sher, A. V., Virina, E. I. & Zazhigin, V. S. Stratigraphy, paleomagnetism, and mammal fauna of the Pliocene--Pleistocene deposits of the Lower Kolyma River. in *Dokl. Akad. Nauk SSSR* vol. 234 1171–1175 (1977).
10. Sher, A. V. Olyorian land mammal age of northeastern Siberia. *Palaeontographica Italica* **74**, 97–112 (1986).
11. Zazhigin, V. S., Edwards, M. E., Sher, A. V. & Guthrie, R. D. Late-Pliocene and Pleistocene rodent faunas in the Kolyma Lowland: possible correlations with North America. *Terrestrial Paleoenvironmental Studies in Beringia (Edwards ME, Sher AV & Guthrie RD, eds)* 25–29 (1997).
12. Baranova, Y. P. & Biske, S. F. Paleoclimates of the Paleogene and Neogene in Northeastern Asia. *Kontinental'nye tretichnye tolshchi Severo-Vostoka Azii* 86–94 (1979).
13. Painter, T. J. Lindow man, tollund man and other peat-bog bodies: The preservative and antimicrobial action of Sphagnan, a reactive glycuronoglycan with tanning and sequestering properties. *Carbohydr. Polym.* **15**, 123–142 (1991).
14. Virina, E. I., Edwards, M. E., Sher, A. V. & Guthrie, R. D. Paleomagnetic stratigraphy of Pliocene/Pleistocene sediments of the Kolyma Lowland and some problems of correlation with the Alaska record. *Terrestrial Paleoenvironmental Studies in Beringia (Edwards ME, Sher AV & Guthrie RD, eds)* 19–24 (1997).
15. Zazhigin, V. S. Late Pliocene and Anthropogene rodents of the south of western Siberia. *Academy of Sciences of the USSR, Transactions* **339**, 1–156 (1980).

16. Zazhigin, V. S. Complexes of the small mammals of the Late Pliocene-Early Pleistocene of the south of the West Siberia. in *Fundamental problems of the Quaternary: Results of the studies and main directions of future research. Material of the 6th All-Russia Conference of the Study of Quaternary, November 19--23, 2009* 218–220 (Siberian Branch of the Russian Academy of Sciences Novosibirsk, Russia, 2009).
17. Zykin, V. S., Zazhigin, V. S. & Kazanskii, A. Y. The Late Neogene of Southern West Siberian Plains: Stratigraphy, Palaeomagnetism, and the Major Climatic Events. *Geol. Geofiz.* **32**, 78 (1991).
18. Tesakov, A. S. & van Kolfschoten, T. The Early Pleistocene Mimomys hordijki (Arvicolinae, Rodentia) from Europe and the origin of modern neartctic sagebrush voles (Lemmiscus). *Palaeontol. Electronica* **14**, 1–11 (2011).
19. van Kolfschoten, T. The Pleistocene mammalian faunas from the Zuurland boreholes at Brielle, The Netherlands. *Mededelingen van de Werkgroep voor Tertiaire en Kwartaire Geologie* **25**, 73–86 (1988).
20. van Kolfschoten, T., Tesakov, A. S. & Bell, C. J. The first record of Phenacomys (Mammalia, Rodentia, Cricetidae) in Europe (early Pleistocene, Zuurland, The Netherlands). *Quat. Sci. Rev.* **192**, 274–281 (2018).
21. Tesakov, A. S. Biostratigraphy of Middle Pliocene--Eopleistocene of Eastern Europe (based on small mammals). *Biostratigrafiâ srednego pliocena--eopleistocena Vostočnoj Evropy po melkim mlekopitaûŝim* (2004).
22. Westgate, J. A. *et al.* Tephrochronology, magnetostratigraphy and mammalian faunas of Middle and Early Pleistocene sediments at two sites on the Old Crow River, northern Yukon Territory, Canada. *Quaternary Research* vol. 79 75–85 (2013).
23. Guthrie, R. D. & Matthews, J. V. The Cape Deceit Fauna—Early Pleistocene Mammalian Assemblage from the Alaskan Arctic. *Quat. Res.* **1**, 474–510 (1971).
24. Brigham-Grette, J. & Hopkins, D. M. The first paleomagnetic evidence from Cape Deceit: a critical Late Pliocene--early Pleistocene mammal, plant macrofossil, and beetle locality in central Beringia. in *Geological Society of America Abstracts with Programs* vol. 23 A99 (1991).
25. Storer, J. E. The Eastern Beringian vole Microtus deceitensis (Rodentia, Muridae, Arvicolinae) in Late Pliocene and Early Pleistocene faunas of Alaska and Yukon. *Quat. Res.* **60**, 84–93 (2003).
26. Repenning, C. A. *Allophaiomys and the Age of the Olyor Suite, Krestovka Sections, Yakutia*. (U.S. Government Printing Office, 1992).
27. Jackson, L. E., Jr, Barendregt, R. W., Baker, J. & Irving, E. Early Pleistocene volcanism and glaciation in central Yukon: a new chronology from field studies and paleomagnetism. *Can. J. Earth Sci.* **33**, 904–916 (1996).
28. Westgate, J. A. *et al.* Dating Early and Middle (Reid) Pleistocene Glaciations in Central Yukon by Tephrochronology. *Quat. Res.* **56**, 335–348 (2001).
29. Blinov, A. *et al.* Ratio of 36 Cl/Cl in ground ice of east Siberia and its application for chronometry : Ratio of 36 Cl/Cl in ground east Siberia. *Geochem. Geophys. Geosyst.* **10**, (2009).

30. Minyuk, P. S. & Ivanov, Y. Y. The Brunhes-Matuyama boundary in Western Beringia: a review. *Quat. Sci. Rev.* **30**, 2054–2068 (2011).
31. Maglio, V. J. Origin and Evolution of the Elephantidae. *Transactions of the American Philosophical Society* **63**, 1–149 (1973).
32. Lister, A. M., Sher, A. V., van Essen, H. & Wei, G. The pattern and process of mammoth evolution in Eurasia. *Quaternary International* vols 126-128 49–64 (2005).
33. Dabney, J. *et al.* Complete mitochondrial genome sequence of a Middle Pleistocene cave bear reconstructed from ultrashort DNA fragments. *Proc. Natl. Acad. Sci. U. S. A.* **110**, 15758–15763 (2013).
34. Meyer, M. & Kircher, M. Illumina sequencing library preparation for highly multiplexed target capture and sequencing. *Cold Spring Harb. Protoc.* **2010**, db.prot5448 (2010).
35. Pečnerová, P. *et al.* Mitogenome evolution in the last surviving woolly mammoth population reveals neutral and functional consequences of small population size. *Evol Lett* **1**, 292–303 (2017).
36. Gansauge, M.-T. & Meyer, M. Single-stranded DNA library preparation for the sequencing of ancient or damaged DNA. *Nat. Protoc.* **8**, 737–748 (2013).
37. Korlević, P. *et al.* Reducing microbial and human contamination in DNA extractions from ancient bones and teeth. *Biotechniques* **59**, 87–93 (2015).
38. Basler, N. *et al.* Reduction of the contaminant fraction of DNA obtained from an ancient giant panda bone. *BMC Res. Notes* **10**, 754 (2017).
39. Paijmans, J. L. A. *et al.* Sequencing single-stranded libraries on the Illumina NextSeq 500 platform. *arXiv [q-bio.OT]* (2017).
40. Palkopoulou, E. *et al.* A comprehensive genomic history of extinct and living elephants. *Proc. Natl. Acad. Sci. U. S. A.* **115**, E2566–E2574 (2018).
41. John, J. S. SeqPrep: Tool for stripping adaptors and/or merging paired reads with overlap into single reads. *URL: https://githubcom/jstjohn/SeqPrep* (2011).
42. Palkopoulou, E. *et al.* Complete genomes reveal signatures of demographic and genetic declines in the woolly mammoth. *Curr. Biol.* **25**, 1395–1400 (2015).
43. Schubert, M. *et al.* Improving ancient DNA read mapping against modern reference genomes. *BMC Genomics* **13**, 178 (2012).
44. Li, H. Aligning sequence reads, clone sequences and assembly contigs with BWA-MEM. *arXiv [q-bio.GN]* (2013).
45. Li, H. *et al.* The Sequence Alignment/Map format and SAMtools. *Bioinformatics* **25**, 2078–2079 (2009).
46. Quinlan, A. R. BEDTools: the Swiss-army tool for genome feature analysis. *Curr. Protoc. Bioinformatics* **47**, 11–12 (2014).
47. Feuerborn, T. R. *et al.* Competitive mapping allows to identify and exclude human DNA contamination in ancient faunal genomic datasets. *bioRxiv* 2020.03.05.974907 (2020) doi:10.1101/2020.03.05.974907.
48. Jónsson, H., Ginolhac, A., Schubert, M., Johnson, P. L. F. & Orlando, L. mapDamage2.0: fast approximate Bayesian estimates of ancient DNA damage parameters. *Bioinformatics* **29**, 1682–1684 (2013).

49. de Filippo, C., Meyer, M. & Prüfer, K. Quantifying and reducing spurious alignments for the analysis of ultra-short ancient DNA sequences. *BMC Biol.* **16**, 121 (2018).
50. Green, R. E. *et al.* A draft sequence of the Neandertal genome. *Science* **328**, 710–722 (2010).
51. Briggs, A. W. *et al.* Removal of deaminated cytosines and detection of in vivo methylation in ancient DNA. *Nucleic Acids Res.* **38**, e87 (2010).
52. Skoglund, P. *et al.* Separating endogenous ancient DNA from modern day contamination in a Siberian Neandertal. *Proc. Natl. Acad. Sci. U. S. A.* **111**, 2229–2234 (2014).
53. Green, R. E. *et al.* A complete Neandertal mitochondrial genome sequence determined by high-throughput sequencing. *Cell* **134**, 416–426 (2008).
54. Rohland, N. *et al.* Proboscidean mitogenomics: chronology and mode of elephant evolution using mastodon as outgroup. *PLoS Biol.* **5**, (2007).
55. Krause, J. *et al.* Multiplex amplification of the mammoth mitochondrial genome and the evolution of Elephantidae. *Nature* **439**, 724–727 (2006).
56. Edgar, R. C. MUSCLE: multiple sequence alignment with high accuracy and high throughput. *Nucleic Acids Res.* **32**, 1792–1797 (2004).
57. Chang, D. *et al.* The evolutionary and phylogeographic history of woolly mammoths: a comprehensive mitogenomic analysis. *Sci. Rep.* **7**, 44585 (2017).
58. Meyer, M. *et al.* Palaeogenomes of Eurasian straight-tusked elephants challenge the current view of elephant evolution. *Elife* **6**, (2017).
59. Darriba, D., Taboada, G. L., Doallo, R. & Posada, D. jModelTest 2: more models, new heuristics and parallel computing. *Nat. Methods* **9**, 772 (2012).
60. Hasegawa, M., Kishino, H. & Yano, T. Dating of the human-ape splitting by a molecular clock of mitochondrial DNA. *J. Mol. Evol.* **22**, 160–174 (1985).
61. Yang, Z. Maximum likelihood phylogenetic estimation from DNA sequences with variable rates over sites: approximate methods. *J. Mol. Evol.* **39**, 306–314 (1994).
62. Suchard, M. A. *et al.* Bayesian phylogenetic and phylodynamic data integration using BEAST 1.10. *Virus Evol* **4**, vey016 (2018).
63. Gill, M. S. *et al.* Improving Bayesian population dynamics inference: a coalescent-based model for multiple loci. *Mol. Biol. Evol.* **30**, 713–724 (2013).
64. Rambaut, A., Drummond, A. J., Xie, D., Baele, G. & Suchard, M. A. Posterior Summarization in Bayesian Phylogenetics Using Tracer 1.7. *Syst. Biol.* **67**, 901–904 (2018).
65. Meyer, M. *et al.* A high-coverage genome sequence from an archaic Denisovan individual. *Science* **338**, 222–226 (2012).
66. Lefort, V., Desper, R. & Gascuel, O. FastME 2.0: A Comprehensive, Accurate, and Fast Distance-Based Phylogeny Inference Program. *Mol. Biol. Evol.* **32**, 2798–2800 (2015).
67. Kumar, S., Stecher, G., Li, M., Knyaz, C. & Tamura, K. MEGA X: Molecular Evolutionary Genetics Analysis across Computing Platforms. *Mol. Biol. Evol.* **35**, 1547–1549 (2018).
68. Patterson, N. *et al.* Ancient admixture in human history. *Genetics* **192**, 1065–1093 (2012).
69. Kimura, M. & Ohta, T. The Average Number of Generations until Fixation of a Mutant Gene in a Finite Population. *Genetics* **61**, 763–771 (1969).
70. Prüfer, K. *et al.* The complete genome sequence of a Neanderthal from the Altai Mountains.

Nature **505**, 43–49 (2014).
71. Barlow, A. *et al.* Partial genomic survival of cave bears in living brown bears. *Nat Ecol Evol* **2**, 1563–1570 (2018).
72. Lister, A. M. Dating the arrival of straight-tusked elephant (Palaeoloxodon spp.) in Eurasia. *Bulletin Du Musée d'anthropologie Préhistorique De Monaco* **6**, 123–128 (2016).
73. Leppälä, K., Nielsen, S. V. & Mailund, T. admixturegraph: an R package for admixture graph manipulation and fitting. *Bioinformatics* **33**, 1738–1740 (2017).
74. Liu, L. *et al.* Genomic analysis on pygmy hog reveals extensive interbreeding during wild boar expansion. *Nat. Commun.* **10**, 1992 (2019).
75. Pickrell, J. K. & Pritchard, J. K. Inference of population splits and mixtures from genome-wide allele frequency data. *PLoS Genet.* **8**, e1002967 (2012).
76. Skov, L. *et al.* Detecting archaic introgression using an unadmixed outgroup. *PLoS Genet.* **14**, e1007641 (2018).
77. Frith, M. C., Hamada, M. & Horton, P. Parameters for accurate genome alignment. *BMC Bioinformatics* **11**, 80 (2010).
78. McLaren, W. *et al.* The Ensembl Variant Effect Predictor. *Genome Biol.* **17**, 122 (2016).
79. Fry, E. *et al.* Functional Architecture of Deleterious Genetic Variants in the Genome of a Wrangel Island Mammoth. *Genome Biol. Evol.* **12**, 48–58 (2020).
80. Lynch, V. J. *et al.* Elephantid Genomes Reveal the Molecular Bases of Woolly Mammoth Adaptations to the Arctic. *Cell Rep.* **12**, 217–228 (2015).
81. Eden, E., Navon, R., Steinfeld, I., Lipson, D. & Yakhini, Z. GOrilla: a tool for discovery and visualization of enriched GO terms in ranked gene lists. *BMC Bioinformatics* **10**, 48 (2009).
82. Yang, Z. PAML 4: phylogenetic analysis by maximum likelihood. *Mol. Biol. Evol.* **24**, 1586–1591 (2007).
83. Cunningham, F. *et al.* Ensembl 2019. *Nucleic Acids Res.* **47**, D745–D751 (2019).
84. Kumar, S., Stecher, G., Suleski, M. & Hedges, S. B. TimeTree: A Resource for Timelines, Timetrees, and Divergence Times. *Mol. Biol. Evol.* **34**, 1812–1819 (2017).